International Journal of Biological Macromolecules 344 (2026) 150373

Contents lists available at ScienceDirect

International Journal of Biological Macromolecules

journal homepage: www.elsevier.com/locate/ijbiomac

Formulating white rice with low–glycemic index potential: The effect of low–acyl gellan gum on textural properties and starch digestibility reduction

Qingsu Liu [a], Vincenzo Di Bari [a,*], Nicholas James Watson [b]

[a] Division of Food, Nutrition and Dietetics, School of Biosciences, University of Nottingham, Sutton Bonington Campus, Loughborough, LE12 5RD, UK
[b] School of Food Science and Nutrition, University of Leeds, Leeds, LS2 9JT, UK

ARTICLE INFO

Keywords:
White rice
Low–acyl gellan gum
Protein–starch matrix
Starch digestibility
Predicted glycemic index

ABSTRACT

White rice is a staple food worldwide, yet its high glycemic index (GI), driven by rapidly digestible starch, raises significant public health concerns.

This study explores the application of low–acyl gellan gum (LAGG) as a bio–macromolecular strategy to modulate starch digestibility while preserving desirable textural properties in cooked rice. Two rice types, jasmine rice (JR, high–GI) and parboiled rice (PR, low–GI), were cooked with 0–3% LAGG and systematically analyzed using a multi–scale approach, including thermal properties at grain and starch levels, microstructural features in raw and cooked forms, and texture and digestibility at the whole grain level, reflecting typical consumption conditions.

Microstructural evaluation of cooked rice revealed that LAGG formed a hydrogel coating on rice grains, enhanced β–sheet protein structures and promoted the formation of starch–LAGG complexes. These structural modifications strengthened the protein–starch matrix, particularly in JR. As a result, hardness (8–26%) and chewiness (1.4–2.3×) increased in JR, while minimal effects were observed in PR. In–vitro starch digestibility analysis showed that LAGG addition reduced starch hydrolysis, shifting digestion toward slower and resistant fractions and lowering predicted GI by 10–22% across LAGG levels (1–3%), with JR showing a stronger response. When integrated with microstructural and thermal observations, these results are consistent with reduced enzymatic accessibility to starch.

Collectively, these findings offer mechanistic insights into LAGG as a distinct hydrocolloid capable of reinforcing rice structure and lowering glycemic impact through multi–scale interactions, supporting its practical and scalable application in the development of healthier rice–based foods.

1. Introduction

White rice remains a fundamental component of the global diet, contributing up to 20% of global caloric intake and as much as 50% in certain Asian regions [1]. However, its high glycemic index (GI), driven by rapidly digestible starch, is associated with an increased risk of type 2 diabetes and imposes substantial public health pressures and costs [2,3]. As public health strategies increasingly focus on dietary GI reduction, developing lower–GI rice products without compromising sensory qualities has become a pressing nutritional challenge [4].

Existing approaches to reduce rice GI – such as genetic, enzymatic, chemical, and physical modifications [5,6] – often involve high costs, complex processing, or undesirable changes in texture and flavor [7,8]. Substituting white rice with lower–GI alternatives like brown rice or konjac rice, frequently faces low consumer acceptance due to altered mouthfeel and eating quality [9]. Thus, there is a growing interest in scalable, ingredient–based approaches that preserve rice's textural profile while improving its nutritional functionality.

Hydrocolloids are widely explored for reducing starch for GI modulation because their physicochemical and structural behavior within food matrices can govern starch gelatinization and enzymatic accessibility [10]. Most commonly used hydrocolloids reduce starch digestibility through bulk–phase effects, including viscosity–driven diffusion control (e.g., xanthan and guar gum) or hydration–induced

* Corresponding author.
E-mail address: vincenzo.dibari@nottingham.ac.uk (V. Di Bari).

https://doi.org/10.1016/j.ijbiomac.2026.150373
Received 26 September 2025; Received in revised form 29 December 2025; Accepted 17 January 2026
Available online 19 January 2026

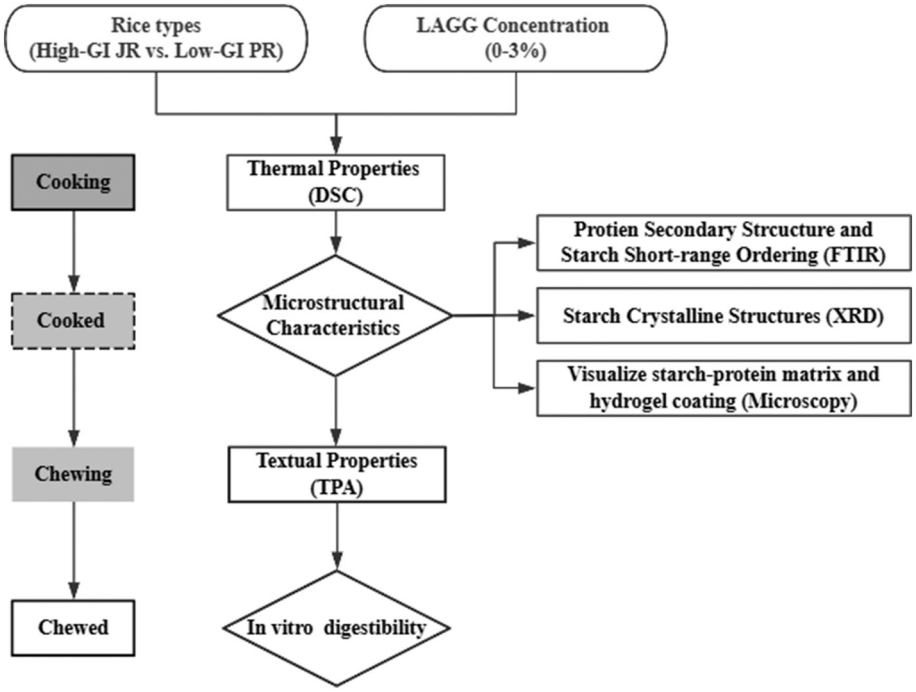

Fig. 1. The methodology employed in the study.

matrix swelling that increases diffusion distances (e.g., konjac glucomannan and carboxymethyl cellulose), thereby delaying enzymatic access [11–14]. Gellan gum differs from these hydrocolloids in that its effect on slowing starch digestibility is associated with localized interfacial structuring, involving hydrogel coatings at the grain or starch surface rather than predominantly bulk–phase viscosity. Within gellan gums, acyl content further determines gel structure and functionality. High acyl gellan gum forms soft, elastic gels with high water retention, which primarily influence food texture and may also provide limited resistance to enzymatic access. In contrast, low–acyl gellan gum (LAGG), with fewer O–acyl substituents (and thus reduced interchain steric hindrance), forms thinner, firmer coating layers structures with pH– and ion–responsive stability [15]. These properties enable LAGG–derived interfacial structures to persist under gastric conditions and potentially limit starch hydrolysis during subsequent intestinal digestion. As such, LAGG exhibits a distinct structure–function relationship among hydrocolloids, supporting its selection in this study.

However, the multi–scale interactions between hydrocolloids and rice components—spanning molecular level bonding, meso–scale matrix formation, and macro–structural changes in texture and digestibility—are still not well comprehended. While the effects of LAGG on isolated rice starch have been partially characterized, its interactions with the native protein–starch matrix during and after cooking remain largely unexplored. Elucidating how LAGG modulates rice structure across hierarchical levels—from molecular organization to whole grain architecture—may provide a mechanistic foundation for the development of functional, lower–GI rice products.

This study investigates the functional potential of LAGG in modulating starch digestibility in cooked white rice, aiming to bridge structural modification with nutritional improvement. We hypothesize that incorporating LAGG during rice cooking alters the protein–starch matrix and reduces enzymatic digestibility while maintaining acceptable textural properties. Two commercially available white rice models with distinct glycemic characteristics and high market prevalence in the UK were selected [2,16,17]: jasmine rice (JR; conventual–processed, high–GI, 89 > 70) and parboiled long–grain white rice (PR; hydrothermal–processed low–GI 47 < 55). The parboiled rice, also marketed as “easy–cook long–grain white rice,” is produced from the same *Indica* cultivar group as JR and has comparable starch content and grain morphology. The main distinction proposes to its internal organization and digestibility, as parboiling induces starch retrogradation and protein–starch reassembly, collectively lowering its starch digestibility and glycemic response. This makes PR a suitable low–GI comparator for assessing LAGG effects across rice systems with comparable botanical origins but distinct intrinsic structures and baseline digestibility. The selected LAGG range (1–3% *w/w*) was guided by preliminary formulation trials, in which levels below 1% produced no measurable changes in starch digestibility, whereas concentrations above 3% substantially increased cooking medium viscosity, impairing rice immersion and uniform gelatinization under standard cooking conditions. The 1–3% range therefore represents a practical formulation window compatible with conventional rice processing, limited ingredient loading, and minimal risk of adverse textural effects.

Building on this, the study integrates multi–scale analyses—spanning starch, flour, and grain levels—to link LAGG–induced molecular and microstructural changes with their impact on texture and in–vitro starch digestibility. This framework provides mechanistic insight into hydrocolloid–mediated matrix assembly and demonstrates a practical route for producing lower–GI rice–based foods without compromising consumer–relevant texture.

2. Materials and methods

2.1. Materials

Jasmine white rice (JR; long–grain *Indica* variety) and parboiled long–grain white rice (PR; long–grain *Indica* variety) were purchased from Tesco, Nottingham, UK, in November 2022. In–house measurements confirmed the pGI of intact JR (71.5 ± 3.8) and PR (50.0 ± 1.6) grains, consistent with reported high– and low–GI classifications, respectively. Low–acyl gellan gum (LAGG) was obtained from CP Kelco, UK. Enzymes for in–vitro digestion, including α–amylase (A–1031), pepsin (P–7000), and pancreatin (P1750), were purchased from Sigma–Aldrich. Enzyme activity validation was performed according to INFOGEST protocols [18], with detailed procedures provided therein. All reagents were of analytical grade unless otherwise specified.

Table 1
Sample codes, material types, and analytical techniques used in the study.

Sample code	Material	Type	Analyses performed
JRS	Jasmine rice isolated starch	Starch	DSC, FTIR, XRD
PRS	Parboiled rice isolated starch	Starch	DSC, FTIR, XRD
JRF	Jasmine rice flour	Flour	Microscopy
PRF	Parboiled rice flour	Flour	Microscopy
JR_xLAGG	JR grain cooking with 0–3% LAGG	Grain	DSC, microscopy, TPA, In–vitro digestion
PR_xLAGG	PR grain cooking with 0–3% LAGG	Grain	DSC, microscopy, TPA, In–vitro digestion
JR_xLAGG_F	JR Grain cooked with 0–3% LAGG, then ground to flour	Flour	FTIR, XRD
PR_xLAGG_F	PR Grain cooked with 0–3% LAGG, then ground to flour	Flour	FTIR, XRD

Table 2
Proximate composition of JR and PR flours and their isolated starches (g/100 g, as–is basis including native moisture).

	Moisture content	Total starch	Amylose	Protein
JRS	2.43 ± 0.35^{b}	95.60 ± 1.32^{a}	18.03 ± 1.79^{b}	0.62 ± 0.03^{c}
JR	8.59 ± 0.04^{a}	83.63 ± 1.68^{b}	17.19 ± 0.08^{b}	6.66 ± 0.58^{b}
PRS	2.60 ± 0.39^{b}	95.02 ± 0.58^{a}	28.84 ± 1.68^{a}	0.65 ± 0.02^{c}
PR	8.24 ± 0.02^{a}	81.68 ± 1.32^{b}	27.01 ± 0.78^{a}	8.52 ± 0.26^{a}

Values are means ± standard deviation. Within each column, values denoted by the same letter are not significantly different ($p > 0.05$).

2.2. Methods overview

The study evaluated the impact of LAGG on starch digestibility and structural properties in two rice types (JR and PR). A schematic overview of sample types, treatments, and analytical methods is presented in Fig. 1. Table 1 summarizes the sample codes used throughout the study.

Each code reflects the rice sample (JR or PR), treatment level (x = 0, 1, 2, or 3 depending on LAGG concentration), and structural form – starch (S), flour (F), or whole grain. These designations allow clear tracking of treatment effects across analytical techniques. Corresponding analyses included thermal (DSC), structural (FTIR, XRD), microstructural (microscopy), texture profile (TPA), and in–vitro digestibility assays.

2.3. Preparation and cooking

2.3.1. Preparation of flour and isolated starch

Cleaned rice grains (100 g) were ground using an electric grinder (KG49, DeLonghi, Treviso, Italy) and sieved to obtain flour with particle sizes <500 μm. The resulting samples were labeled as JRF (Jasmine rice flour) and PRF (Parboiled rice flour), respectively. Starch was isolated following the method described previously [19]: 50 g flour was dispersed in 0.18% NaOH (1:15 *w/v* ratio) at 30 °C for 1 h. After centrifugation using a benchtop centrifuge (Rotina 380, Hettich GmbH, Tuttlingen, Germany) at 3100 ×*g* for 15 min, the protein–rich supernatant was removed. The pellet was neutralized with 0.1 M HCl, washed with distilled water, and dried at 30 °C to constant weight in a forced–air oven (MOV-112F, Sanyo, Japan). The dried material was then milled and sieved (<500 μm). The resulting isolated starches were labeled as JRS (Jasmine rice starch) and PRS (Parboiled rice starch), respectively.

2.3.2. Preparation of cooked rice grain with LAGG and starch–LAGG systems

Washed rice grains (100 g) were cooked in a rice cooker (NEDIS, Karc06wt, 300 W, Leicester, UK) with a 1:1.5 (*w/v*) rice–to–liquid ratio for approximately 15 min, followed by a warming phase (10 min) at 65–70 °C. Control samples were cooked in water alone; while treated samples were cooked in LAGG–water dispersions (1, 2, or 3 g – contained in the 150 mL liquid–/100 g dry rice). Complete cooking was verified by compressing 10 randomly selected grains from the center of the cooking pot between glass slides; the absence of an opaque core indicated complete gelatinization. Freshly cooked grains were divided for analysis: one portion was used immediately for TPA, while the remaining portion was snap–frozen in liquid nitrogen to preserve microstructure, then freeze–dried, milled (<500 μm), and stored at −20 °C. Resulting flours were labeled JR_xLAGG_F and PR_xLAGG_F, where x (0–3) denotes LAGG concentration (*w/w*).

Starch isolates (JRS and PRS) were used to prepare starch–LAGG systems for comparison. LAGG was incorporated directly into starch isolates at concentrations equivalent to those used in the rice grain systems, calculated on a starch–weight basis. Specifically, 1%, 2%, and 3% LAGG relative to total rice weight corresponded to approximately 1.2%, 2.4%, and 3.6% LAGG relative to starch–weight (95% purity), respectively, based on the assumption that starch accounts for 82–83% of the dry matter in both JR and PR. To maintain consistency with the rice grain formulations, starch–LAGG mixtures were labeled using the same notation), e.g., JRS_1LAGG (eq.), where "(eq.)" indicates equivalent LAGG levels corresponding to the respective rice systems.

2.4. Proximate composition analysis of rice samples

Proximate composition was analyzed using AOAC standard methods. Moisture content was determined by drying 2 g of each sample at 105 °C to constant weight (AOAC 934.01). Crude protein was measured using the Kjeldahl method with a 5.95 nitrogen–to–protein conversion factor (AOAC 930.29). Total starch and amylose content were quantified using Megazyme kits (AOAC 996.11 K–TSTA and K–AMYL; Megazyme, Ireland). All measurements were performed in triplicate and reported as mean ± standard deviation.

2.5. Protein extraction and electrophoresis

Protein extraction and electrophoresis were conducted to assess the extent of disulfide–linked protein crosslinking and its modulation by LAGG during rice cooking. Freeze–dried rice powder was homogenized in SDS buffer (50 mM Tris–HCl, pH 7.5, 2% SDS, 10% glycerol, 0.01% bromophenol blue), with or without 5% β–mercaptoethanol (reducing vs. non–reducing conditions). After heating at 95 °C (10 min) and centrifugation (10,000 ×*g*, 10 min), supernatants were loaded onto 12% SDS–PAGE gels (Mini–PROTEAN, Bio–Rad). Gels were stained with Coomassie Brilliant Blue and banding patterns compared under reducing/non–reducing conditions to assess disulfide–linked crosslinking.

2.6. Thermal properties (DSC)

Thermal transitions of rice grain and starch were analyzed using a differential scanning calorimeter (DSC^{3+}, Mettler Toledo, Leicester, UK) adapted from method [20] to simulate the rice cooker condition. 10 mg rice kernel sections or starch–equivalent to 10 mg rice were mixed with 15 μL distilled water or LAGG dispersion, sealed in pans (40 μL), and heated from 30 °C to 120 °C at 10 °C/min. After holding at 120 °C (15 min), samples were cooled to 60 °C at 20 °C/min. Thermal parameters – onset (T_o), peak (T_p), end (T_e) temperature, and enthalpy changes (ΔH) – were calculated using $STAR^e$ software (Mettler Toledo, Leicester, UK). All measurements were performed in triplicate. The ΔH was normalized to starch content on a dry–weight basis.

2.7. Microstructural analysis

2.7.1. FTIR spectroscopy

FTIR spectra of raw and cooked samples were obtained using a Bruker Tensor 27 spectrometer (Graseby Space Ltd., Orpington, UK) following the method [21]. Spectra were recorded in the 4000–400 cm^{-1} range (128 scans, 4 cm^{-1} resolution), with ambient air serving as

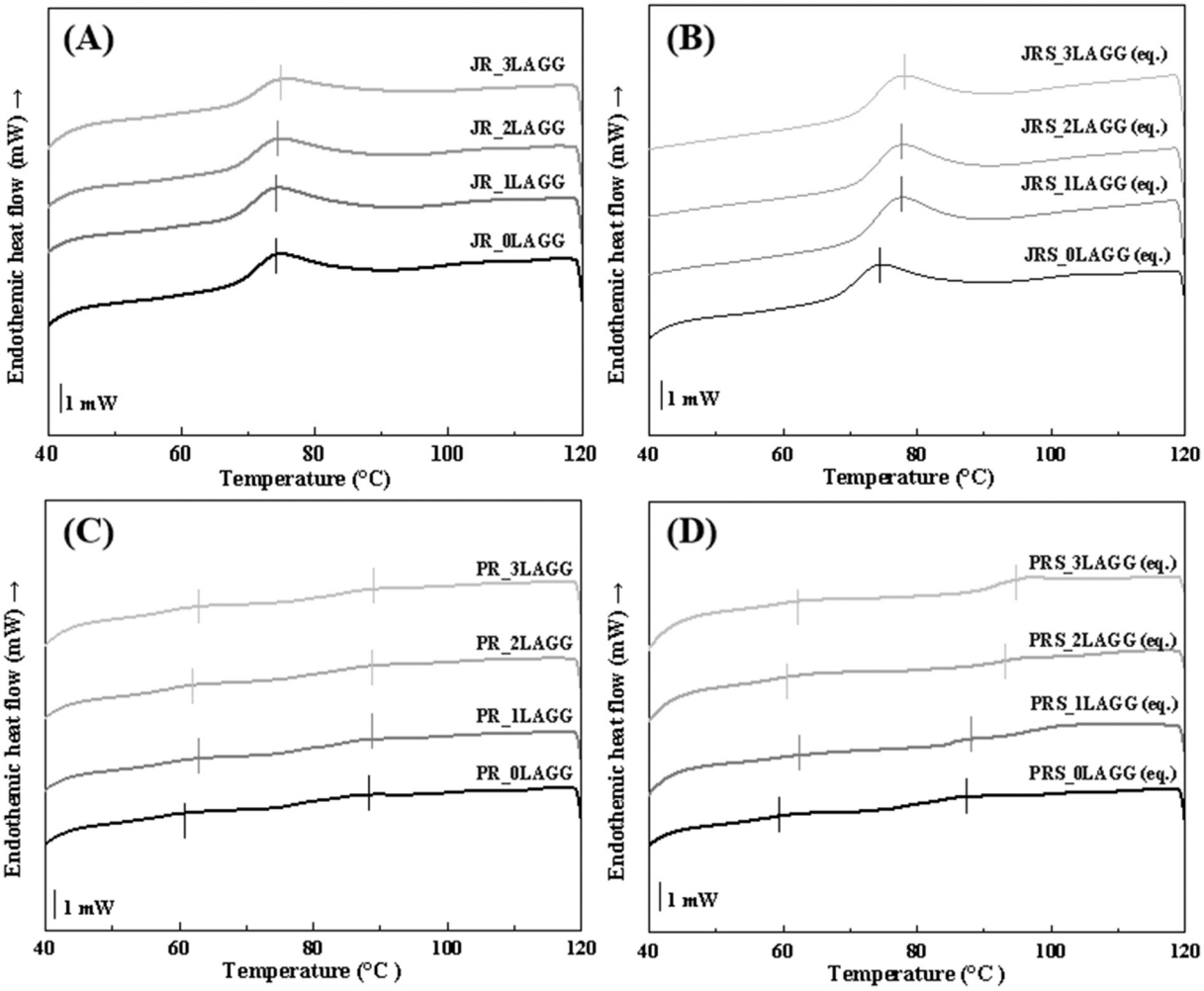

Fig. 2. DSC thermograms were obtained for JR (A), JRS (B), PR (C), and PRS (D) heating in 0–3% LAGG–water dispersions. The endothermic heat flow was measured for samples subjected to heating from 30 to 120 °C at a rate of 10 °C/min, thereby simulating the conditions typically encountered in a rice cooker. Rice flour (either JR or PR) and starch isolates (designated as JRS or PRS) were incorporated into LAGG aqueous dispersions at concentrations of 0, 1, 2, or 3% (*w*/w), while maintaining a mass–to–dispersion ratio of 1:1.5. Starch–LAGG samples are labeled consistently with the grain samples, with "(eq.)" indicating LAGG levels equivalent to the grain formulations.

the background reference. Data analysis was performed using the OMNIC software (version 6.2, Thermo Electron Corporation). After baseline correction and spectral deconvolution, the secondary structure of rice proteins, including β–sheet, random coil, α–helix and β–turn, was quantified in the amide I region (1700 cm^{-1} to 1600 cm^{-1}) by Gaussian peak fitting [22]. The percentage contribution of each structural component was calculated by dividing its peak area by the total fitted peak area. Starch short-range molecular order was evaluated using absorbance ratios at 995/1022 and 1047/1022 [23].

2.7.2. X–ray diffraction (XRD)

The crystalline structure was assessed using a Bruker D8 diffractometer (D8, Bruker Ltd., Coventry, UK) with a Cu–Kα radiation source (λ = 0.154 nm) at 40 kV and 25 mA, as in the method outlined by [24]. Samples were scanned from 4° to 45°(2θ) with a step size of 0.02° (2θ) and a scan speed of 2°/min. Degree of crystallinity (DOC) was calculated as the ratio of crystalline peak area to total diffraction area using the DIFFRAC plus EVA® software (Bruker Ltd., Coventry, UK). The loss of crystallinity was calculated using Eq. (1) as:

$$\text{Loss of Crystallinity } (\%) = \frac{DOC_{raw} - DOC_{treated}}{DOC_{raw}} \times 100\% \quad (1)$$

2.7.3. Microstructural and morphological analysis

Brightfield and polarized–light microscopy (Eclipse Ci, Nikon Instruments Inc., Surrey, UK) were used to observe raw rice flour and starch suspensions (1% *w/v*) [25]. Images were recorded at 20× magnification. Particle size distributions were measured using a laser diffraction analyzer (LS 13 320, powder system module, Beckman Coulter, Inc., Buckinghamshire, UK), with a refractive index set to 1.33. The volume–weighted mean diameter $d_{(4,3)}$ was reported as the average of three technical replicates. Grain dimensions (length, width, thickness) were recorded using a digital caliper (0.01 mm resolution; PGA1001, Modelcraft, UK). Cryo–embedded samples were prepared as suggested method [26], sectioned (60 μm) using a Leica CM 3050 s microtome (Leica Microsystems Ltd., Solihull, UK), and stained with 0.1% fast green in acetic acid (protein) and 0.2% Lugol's iodine solution (starch). LAGG was fluorescently labeled with 5–(4,6–dichlorotriazinyl) amino fluorescein (DTAF) labeling [27] and visualized using EVOS™ FL microscope ($\lambda_{Excitation}$ = 488 nm; $\lambda_{Emission}$ = 517 nm). Surface and cross–sectional morphology was captured using an Environmental Scanning Electron Microscope (ESEM, FEI Quanta 650, Thermo Fisher Scientific, Paisley, UK) under the conditions described previously [28].

Table 3
Thermal properties of rice samples upon heating.

Rice type	T_{o1} (°C)	T_{p1} (°C)	T_{e1} (°C)	ΔH_{en1} (J/g of starch)	T_{o2} (°C)	T_{p2} (°C)	T_{e2} (°C)	ΔH_{en2} (J/g of starch)
JRS_0LAGG	64.25 ± 0.72 ^{b}	71.27 ± 0.80 ^{b}	83.63 ± 1.01 ^{a}	9.14 ± 0.42 ^{a}	–	–	–	–
JRS_1LAGG (eq.)	68.69 ± 0.38 ^{a}	75.06 ± 0.23 ^{a}	85.31 ± 0.21 ^{a}	9.27 ± 0.29 ^{a}	–	–	–	–
JRS_2LAGG (eq.)	68.87 ± 0.14 ^{a}	75.36 ± 0.09 ^{a}	85.69 ± 0.30 ^{a}	9.32 ± 0.11 ^{a}	–	–	–	–
JRS_3LAGG (eq.)	68.64 ± 0.07 ^{a}	75.37 ± 0.10 ^{a}	85.58 ± 0.25 ^{a}	9.63 ± 0.23 ^{a}	–	–	–	–
JR_0LAGG	63.30 ± 0.78 ^{b}	70.45 ± 0.94 ^{b}	77.47 ± 1.20 ^{b}	7.19 ± 0.41 ^{b}	–	–	–	–
JR_1LAGG	65.64 ± 0.15 ^{b}	72.94 ± 0.68 ^{b}	78.17 ± 1.31 ^{b}	7.32 ± 0.35 ^{b}	–	–	–	–
JR_2LAGG	65.35 ± 0.79 ^{b}	72.50 ± 0.40 ^{b}	78.96 ± 1.54 ^{b}	7.28 ± 0.21 ^{b}	–	–	–	–
JR_3LAGG	65.44 ± 0.35 ^{b}	71.96 ± 0.59 ^{b}	78.82 ± 1.03 ^{b}	7.45 ± 0.33 ^{b}	–	–	–	–
PRS_0LAGG	49.53 ± 1.16 ^{c}	59.51 ± 0.63 ^{d}	71.97 ± 1.37 ^{d}	0.91 ± 0.11 ^{d}	84.27 ± 0.55 ^{b}	88.89 ± 2.98 ^{ab}	93.48 ± 2.07 ^{ab}	0.52 ± 0.06 ^{a}
PRS_1LAGG (eq.)	51.78 ± 0.96 ^{c}	62.25 ± 0.78 ^{c}	75.47 ± 0.96 ^{c}	1.22 ± 0.12 ^{c}	84.63 ± 0.59 ^{b}	90.17 ± 1.47 ^{a}	94.94 ± 2.27 ^{ab}	0.48 ± 0.02 ^{a}
PRS_2LAGG (eq.)	51.05 ± 0.62 ^{c}	62.30 ± 0.46 ^{c}	75.12 ± 1.71 ^{c}	1.42 ± 0.33 ^{c}	86.08 ± 0.94 ^{ab}	91.68 ± 2.77 ^{a}	95.04 ± 1.29 ^{a}	0.45 ± 0.04 ^{a}
PRS_3LAGG (eq.)	52.39 ± 0.81 ^{c}	63.47 ± 1.29 ^{c}	74.35 ± 0.96 ^{c}	1.30 ± 0.27 ^{c}	88.36 ± 0.97 ^{a}	93.31 ± 2.42 ^{a}	98.22 ± 2.00 ^{a}	0.46 ± 0.04 ^{a}
PR_0LAGG	50.79 ± 1.18 ^{c}	60.26 ± 1.72 ^{d}	72.02 ± 1.72 ^{d}	0.83 ± 0.15 ^{d}	81.68 ± 1.20 ^{c}	87.27 ± 0.72 ^{b}	91.15 ± 0.75 ^{b}	0.26 ± 0.01 ^{b}
PR_1LAGG	51.77 ± 1.17 ^{c}	62.38 ± 1.16 ^{c}	74.54 ± 0.96 ^{c}	0.89 ± 0.25 ^{d}	83.21 ± 1.25 ^{c}	88.63 ± 1.61 ^{ab}	93.70 ± 1.09 ^{b}	0.27 ± 0.02 ^{b}
PR_2LAGG	51.68 ± 0.72 ^{c}	62.50 ± 0.59 ^{c}	73.43 ± 1.08 ^{cd}	1.01 ± 0.10 ^{cd}	84.38 ± 1.97 ^{bc}	89.50 ± 1.56 ^{a}	94.50 ± 1.56 ^{ab}	0.26 ± 0.02 ^{b}
PR_3LAGG	52.08 ± 0.60 ^{c}	63.08 ± 0.34 ^{c}	73.95 ± 1.37 ^{cd}	1.16 ± 0.14 ^{c}	81.12 ± 1.53 ^{c}	87.08 ± 1.34 ^{b}	93.08 ± 1.34 ^{b}	0.30 ± 0.02 ^{b}

Values are means ± standard deviation. Within each column, values denoted by the same letter are not significantly different ($p > 0.05$). $T_{o1\ or\ 2}$: onset temperature; $T_{p\ 1\ or\ 2}$: peak temperature; $T_{e\ 1\ or\ 2}$: end temperature; $\Delta H_{en\ 1\ or\ 2}$: is the enthalpy of gelatinization (J/g of starch on dry–weight basis, dwb). Starch–LAGG samples are labeled consistently with the grain samples, with "(eq.)" indicating LAGG levels equivalent to the grain formulations.

2.8. Textural profile analysis of cooked rice grain

Textural properties of freshly cooked rice were measured using a texture analyzer (TA–XT2, Stable Micro System, Surrey, UK) operated in two–cycle compression mode, following the method [29]. For each sample, 5 g cooked rice grains were gently spread in a single, non–overlapping layer on the sample platform, covering an area exceeding the probe diameter to ensure uniform compression. Samples were compressed using a 35 mm diameter aluminum cylindrical probe at a pre–test speed of 1.0 mm/s, test speed of 1.0 mm/s, and post–test speed of 1.0 mm/s, to a target deformation of 75% strain, with a 5 s interval between compression cycles. A trigger force of 5 g was applied. Ten technical replicates were performed per sample.

Texture parameters–hardness, adhesiveness, cohesiveness, and chewiness–were determined from the resulting force–time curves using Exponent software (Stable Micro Systems, Surrey, UK). Immediately after testing, compressed rice samples were collected for post–compression particle size analysis (d_{50}) to characterize structural fragmentation induced by mechanical deformation, and for subsequent in–vitro digestion assays. Further procedural details are provided in Section 2.9 and Supplementary Materials.

2.9. In–vitro digestion, kinetics of protein and starch digestion, and predicted glycemic indices (pGI)

TPA–tested sample underwent a three–phase in–vitro digestion (oral, gastric, intestinal) as per the INFOGEST rice–specific modifications [30]. Supernatant aliquots were collected after gastric phases and at specific intervals (0, 5, 10, 15, 20, 30, 45, 60, 90, 120, and 180 min) during the intestinal phase for protein and starch hydrolysis analysis. Each sample was tested in triplicate, with two technical replicates per time point. Further procedural details are in the Supplementary Materials.

2.9.1. Starch hydrolysis quantification in cooked rice

The concentration of reducing sugars in the supernatants was quantified using the alkaline p–hydroxybenzoic acid hydrazide (PAHBAH) method [31], with maltose as the standard. The percentage of hydrolyzed starch was calculated based on the amount of reducing sugars released (measured as maltose equivalents) at each time point relative to the total starch content of the sample, expressed on a dry–-weight basis. Moisture content of cooked rice samples was determined gravimetrically prior to analysis, and values were used to normalize all digestion data to eliminate variability due to water uptake during cooking. This approach ensures comparability across treatments with differing hydration levels following Eq. (2) [32].

$$\text{Hydrolyzed starch (\%)} = \frac{\text{Maltose equivalent in the digested supernatant (mg)}}{\text{Total starch content in the sample (maltose equivalents, mg)}} \times 100\% \quad (2)$$

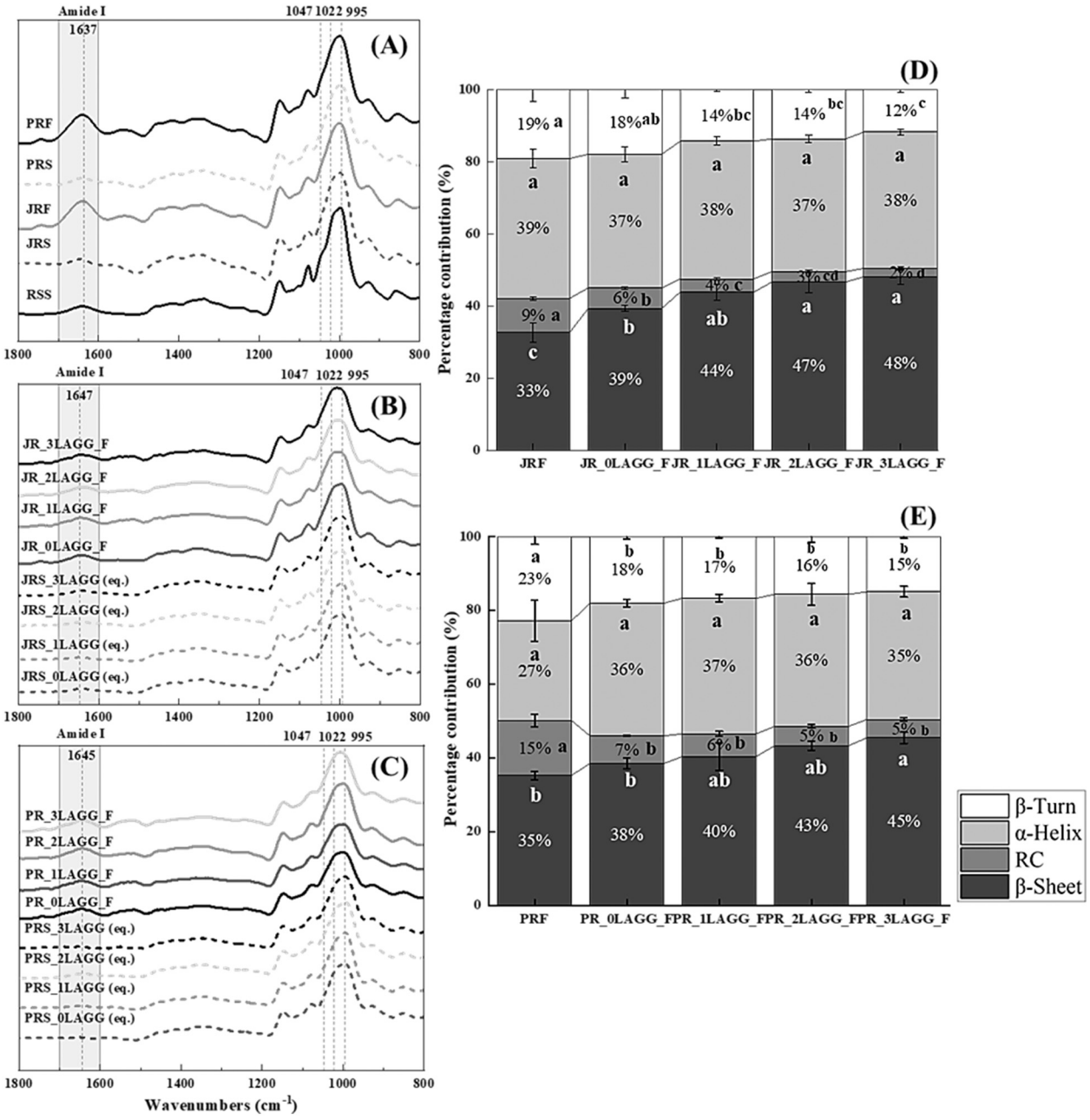

Fig. 3. FTIR spectra and secondary structure analysis of protein in rice samples treated with 0–3% LAGG. (A–C) FTIR spectra of JR, PR, and their starch isolates (JRS, PRS) and LAGG–treated counterparts in the range of 1800–800 cm^{-1}. Amide I peak (1637–1647 cm^{-1}) indicate protein secondary structure changes, while peaks at 995, 1022, and 1047 cm^{-1} reflect starch short–range order. (D, E) Deconvoluted protein secondary structure profiles derived from amide I band fitting, showing relative proportions of β–sheet, random coil (RC), α–helix, and β–turn structures. LAGG addition increased β–sheet content and decreased RC and β–turn fractions, suggesting enhanced protein structural ordering. Starch–LAGG samples are labeled consistently with the grain samples, with "(eq.)" indicating LAGG levels equivalent to the grain formulations. Bars sharing the same letter within each secondary structure (horizontal comparison) are not significantly different ($p > 0.05$).

2.9.2. Protein hydrolysis quantification in cooked rice

Free amino groups were measured using the o–phthaldialdehyde (OPA) method adapted for 96–well microplates, using L–glutamic acid as the standard [33]. Enzyme blanks (enzyme solutions without samples) were subtracted to ensure accurate measurement of sample–derived digestion. The percentages of hydrolyzed protein was determined using Eq. (3), in accordance with the method described previously [34].

$$\text{Hydrolyzed protein (\%)} = \frac{\text{Amino groups in digested supernatant (μmol L – glutamic acid equivalents)}}{\text{Total amino groups in the fully hydrolyzed sample (μmol L – glutamic acid equivalents)}} \times 100\% \quad (3)$$

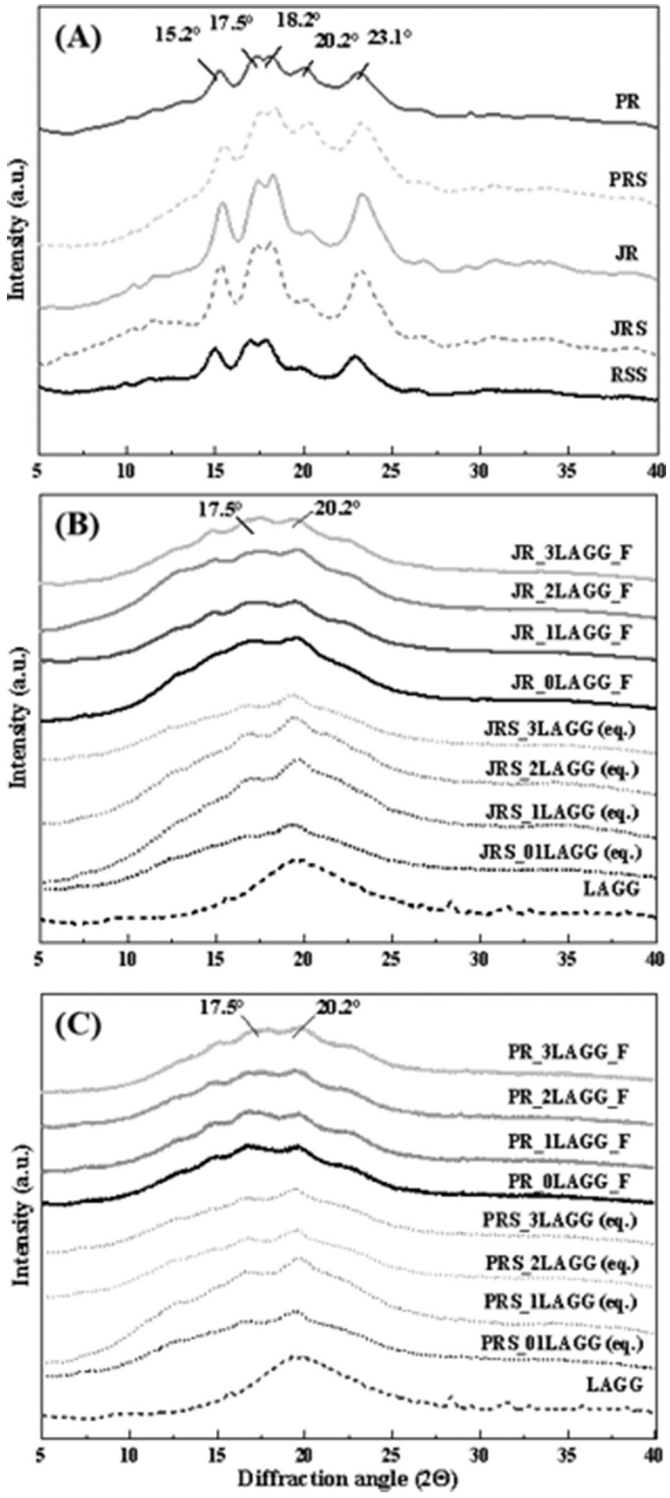

Fig. 4. XRD diffraction patterns. (A) Untreated samples: JR and PR (starch in protein matrix), JRS and PRS (native starch), and RSS (rice starch standard as the reference). (B) Designated as JR and JRS, as well as (C) PR and PRS, were subjected to cooking processes utilizing a LAGG concentration that varied from 0% (control) to 1, 2, and 3% (denoted as 0LAGG, 1LAGG, 2LAGG, and 3LAGG). Starch–LAGG samples are labeled consistently with the grain samples, with "(eq.)" indicating LAGG levels equivalent to the grain formulations.

Table 4
FTIR–derived short–range starch order indicators (995/1022 cm^{-1} and 1047/1022 cm^{-1} band ratios), degree of crystallinity (DOC), and DOC loss in JR and PR treated with 0–3% LAGG.

Rice sample	995/1022	1047/1022	DOC	Loss of DOC
Raw JRS	1.31 ± 0.00 ^{a}	0.37 ± 0.03 ^{a}	12.4 ± 0.4 ^{a}	
JRS_0LAGG	1.15 ± 0.02 ^{c}	0.35 ± 0.02 ^{a}	8.8 ± 0.2 ^{c}	29.03 ± 1.32 ^{ab}
JRS_1LAGG (eq.)	1.06 ± 0.01 ^{d}	0.32 ± 0.01 ^{ab}	8.5 ± 0.1 ^{d}	31.45 ± 0.66 ^{a}
JRS_2LAGG (eq.)	1.04 ± 0.02 ^{de}	0.28 ± 0.03 ^{b}	8.3 ± 0.3 ^{d}	33.06 ± 1.98 ^{a}
JRS_3LAGG (eq.)	1.01 ± 0.02 ^{e}	0.28 ± 0.01 ^{b}	8.0 ± 0.1 ^{e}	35.48 ± 1.96 ^{a}
Raw JRF	1.44 ± 0.02 ^{a}	0.35 ± 0.01 ^{a}	11.3 ± 0.2 ^{b}	
JR_0LAGG_F	1.27 ± 0.03 ^{b}	0.33 ± 0.02 ^{ab}	8.3 ± 0.2 ^{d}	26.55 ± 1.45 ^{b}
JR_1LAGG_F	1.23 ± 0.02 ^{b}	0.29 ± 0.04 ^{b}	7.9 ± 0.3 ^{e}	30.09 ± 2.17 ^{a}
JR_2LAGG_F	1.20 ± 0.03 ^{b}	0.26 ± 0.02 ^{b}	7.8 ± 0.2 ^{e}	30.97 ± 1.45 ^{a}
JR_3LAGG_F	1.01 ± 0.04 ^{c}	0.24 ± 0.01 ^{b}	7.6 ± 0.1 ^{f}	32.74 ± 0.72 ^{a}
Raw PRS	1.25 ± 0.02 ^{b}	0.30 ± 0.02 ^{ab}	8.9 ± 0.3 ^{c}	
PRS_0LAGG	1.16 ± 0.02 ^{c}	0.29 ± 0.01 ^{b}	7.8 ± 0.2 ^{e}	12.36 ± 1.83 ^{d}
PRS_1LAGG (eq.)	1.08 ± 0.01 ^{d}	0.26 ± 0.02 ^{bc}	7.5 ± 0.3 ^{f}	15.73 ± 2.75 ^{c}
PRS_2LAGG (eq.)	1.05 ± 0.02 ^{de}	0.26 ± 0.01 ^{bc}	7.6 ± 0.2 ^{f}	14.61 ± 1.83 ^{cd}
PRS_3LAGG (eq.)	1.05 ± 0.01 ^{de}	0.24 ± 0.01 ^{c}	7.3 ± 0.1 ^{f}	17.98 ± 1.92 ^{c}
Raw PRF	0.98 ± 0.02 ^{c}	0.25 ± 0.03 ^{b}	8.0 ± 0.2 ^{e}	
PR_0LAGG_F	0.88 ± 0.02 ^{d}	0.20 ± 0.02 ^{c}	7.4 ± 0.2 ^{f}	7.50 ± 2.04 ^{e}
PR_1LAGG_F	0.87 ± 0.01 ^{de}	0.18 ± 0.03 ^{c}	7.3 ± 0.2 ^{f}	8.75 ± 1.02 ^{e}
PR_2LAGG_F	0.82 ± 0.07 ^{e}	0.17 ± 0.03 ^{c}	7.1 ± 0.2 ^{g}	11.25 ± 2.04 ^{d}
PR_3LAGG_F	0.80 ± 0.04 ^{e}	0.15 ± 0.02 ^{c}	6.9 ± 0.1 ^{g}	13.75 ± 1.02 ^{d}

Values are mean ± SD ($n = 4$). Within each column, values denoted by the same letter are not significantly different ($p > 0.05$). Starch–LAGG samples are labeled consistently with the grain samples, with "(eq.)" indicating LAGG levels equivalent to the grain formulations.

2.10. Statistical analysis

Data were expressed as mean ± standard deviation. Statistical significance was determined by one–way ANOVA followed by Tukey's post hoc test ($p < 0.05$). Starch and protein hydrolysis kinetics were modeled using first–order equations [35,36]. pGI was calculated from the hydrolysis index (HI) using the equation: pGI = 39.71 + 0.549 × HI [37], with details provided in the Supplementary Materials. Principal component analysis (PCA) was used to identify key contributors to pGI variation, with components retained based on eigenvalues >1. All analyses were performed using SPSS version 27 (SPSS Inc., Chicago, IL, USA).

3. Results and discussions

3.1. Composition and morphology of JR and PR samples

Table 2 summarizes the proximate composition of JR and PR flours and starch isolates. PR flour exhibited higher protein and amylose contents than JR, while total starch and moisture were comparable. Starch isolates (JRS, PRS) showed >95% purity with negligible protein,

Table 5
Proximate composition (g/100 g, wet–weight basis) and morphological properties of cooked JR and PR with 0–3% (*w*/w) LAGG. When normalized to a dry–weight or solids basis, the protein content is consistent with the values reported in Table 2.

Sample	WC (%)	TS (%)	AM (%)	P (%)	L	W	T	Sph	SA	R
JR_0LAGG_F	57.77 ± 2.81 a	35.86 ± 1.92 a	14.26 ± 1.06 b	2.64 ± 0.12 b	1.00 ± 0.03 a	0.30 ± 0.02 a	0.09 ± 0.01 a	0.29 ± 0.02 a	0.53 ± 0.02 a	0.22 ± 0.02 a
JR_1LAGG_F	60.10 ± 2.06 a	35.39 ± 2.17 a	13.73 ± 0.99 b	2.65 ± 0.04 b	1.03 ± 0.05 a	0.30 ± 0.02 a	0.09 ± 0.01 a	0.29 ± 0.02 a	0.57 ± 0.05 a	0.22 ± 0.02 a
JR_2LAGG_F	61.20 ± 1.54 a	34.45 ± 3.46 a	14.12 ± 2.18 b	2.63 ± 0.40 b	0.97 ± 0.05 a	0.30 ± 0.01 a	0.09 ± 0.01 a	0.31 ± 0.01 a	0.54 ± 0.05 a	0.24 ± 0.01 a
JR_3LAGG_F	62.26 ± 1.43 a	35.11 ± 2.61 a	14.69 ± 1.64 b	2.57 ± 0.04 b	1.00 ± 0.06 a	0.32 ± 0.04 a	0.10 ± 0.02 a	0.32 ± 0.04 a	0.60 ± 0.10 a	0.24 ± 0.01 a
PR_0LAGG_F	59.54 ± 2.60 a	33.18 ± 2.27 a	20.19 ± 0.43 a	3.42 ± 0.12 a	1.09 ± 0.03 a	0.32 ± 0.02 a	0.09 ± 0.01 a	0.29 ± 0.02 a	0.64 ± 0.05 a	0.22 ± 0.01 a
PR_1LAGG_F	61.92 ± 1.85 a	31.81 ± 1.56 a	19.48 ± 0.57 a	3.36 ± 0.08 a	0.98 ± 0.07 a	0.28 ± 0.02 a	0.08 ± 0.01 a	0.29 ± 0.02 a	0.50 ± 0.06 a	0.22 ± 0.01 a
PR_2LAGG_F	61.78 ± 1.17 a	32.68 ± 2.42 a	20.13 ± 1.82 a	3.50 ± 0.09 a	0.92 ± 0.03 a	0.30 ± 0.04 a	0.10 ± 0.03 a	0.32 ± 0.05 a	0.52 ± 0.08 a	0.25 ± 0.05 a
PR_3LAGG_F	62.37 ± 1.81 a	32.57 ± 3.32 a	18.89 ± 2.01 a	3.44 ± 0.14 a	0.98 ± 0.04 a	0.28 ± 0.03 a	0.08 ± 0.02 a	0.28 ± 0.03 a	0.50 ± 0.06 a	0.22 ± 0.03 a

Values are means ± standard deviation. Within each column, values denoted by the same letter are not significantly different ($p > 0.05$). WC: water content (g/100 g); TS: total starch (g/100 g); AM: amylose (g/100 g); P: protein (g/100 g); L: length (cm); W: width (cm); T: thickness (cm); Sph: sphericity; SA: surface area (cm^2); R: roundness.

consistent with isolation benchmarks [38].

Microscopy revealed distinct granule morphologies between rice types (Supplementary Fig. 1). JRF displayed compact, polygonal granules with strong birefringence, indicative of well–ordered crystalline regions. PRF showed disrupted birefringence and more aggregated granules, consistent with parboiling–induced structural changes [39]. JRS exhibited discrete angular granules, while PRS retained a clustered morphology despite protein removal.

Particle size distribution (Supplementary Fig. 1, lower panel) showed bimodal peaks for JRS, with the main mode at 4–6 μm, reflecting dispersed granules [40]. In contrast, PRS had a narrower peak and reduced $d_{(4,\ 3)}$ values (310.3 μm), likely due to retrograded starch aggregation rather than protein encapsulation [41].

3.2. Thermal properties and gelatinization behavior of rice samples

DSC analysis revealed distinct thermal behaviors between JR and PR (Fig. 2; Table 3). JR and JRS exhibited well–defined gelatinization peaks between 65 and 84 °C (Fig. 2A, B), while in PR and PRS, no clear melting peaks were observed in the temperature range 55–70 °C (Fig. 2C, D), suggesting intensive thermal treatment during industrial parboiling. This observation aligns with previous findings that higher processing intensity reduces starch melting enthalpy [42,43]. A secondary endothermic transition between 90 and 100 °C, more pronounced in PRS, was likely associated with ungelatinized residual starch granules encased within compact clusters, as shown in Supplementary Fig. 1 (D1 and D2) and possibly with the dissociation of amylose–lipid complexes formed during parboiling [44]. These clusters may impede water penetration and delay the melting of crystalline regions, requiring a higher temperature for gelatinization to occur as observed in the thermographs (Fig. 2D).

LAGG addition (1–3%) elevated gelatinization temperatures and ΔH_{en} particularly in starch isolates (JRS, PRS), indicating stronger LAGG–starch interactions when the protein network was absent. No detectable transitions were observed in LAGG–only controls under the same conditions (data not shown), indicating that thermal effects arose from starch–dependent interchain interactions rather than intrachain rearrangements. These effects were less evident in rice grain level (JR, PR), likely due to steric hindrance by proteins [45].

Upon cooling, weak exothermic peaks (80–90 °C) were observed in JRS and PRS, with higher recrystallization enthalpy (ΔH_c = 1.22 and 1.09 J/g, respectively), compared to JR and PR (<0.85 J/g) (Supplementary Fig. 2, Supplementary Table 1). Although starch retrogradation – particularly in amylopectin–rich varieties like JR – typically occurs at lower temperatures (<60 °C), the elevated onset here may reflect altered molecular dynamics in isolated starch systems. The absence of native structural constraints such as proteins or lipids likely enhances chain mobility and facilitates earlier molecular reordering [46,47]. LAGG suppressed starch restructuring in JRS (rendering ΔH_c undetectable) and reduced ΔH_c in PRS (~0.17–0.20 J/g), while effects in rice grain were negligible. These findings suggest that LAGG more effectively disrupts starch self–restructuring in isolate systems, where its action is less constrained by proteins or structural matrices [48].

3.3. Microstructural properties

3.3.1. Secondary structure of rice protein and short–range starch order

FTIR analysis (Fig. 3) revealed distinct amide I band profiles corresponding to protein secondary structures. PRF had higher random coil (RC) and lower α–helix content than JRF, suggesting the presence of denatured protein, likely resulting from parboiling [49,50]. Upon cooking, amide I peaks shifted from 1637 cm^{-1} to ~1645–1647 cm^{-1}, suggesting protein fragmentation and reorganization [51,52]. This was further supported by SDS–PAGE (Supplementary Fig. 3, non–reducing conditions), which showed high–molecular–weight protein aggregates (~70 kDa) in raw samples – particularly in JR – that were markedly diminished after cooking, indicating heat–induced unfolding and aggregation. LAGG treatment increased β–sheet content while reducing RC in both JR and PR (Fig. 3), indicating enhanced protein ordering. These changes suggest that LAGG may stabilize protein structure, potentially by promoting hydrogen bonding or limiting thermal disruption [53,54].

Starch short–range order was assessed via FTIR band ratios. Higher 995/1022 and 1047/1022 values in raw and cooked JR (vs. PR) indicate greater molecular order, likely due to higher native crystallinity [55,56]. LAGG reduced both ratios across samples, implying disruption of double–helix reformation and retrogradation inhibition [57]. These effects were dose–dependent and more pronounced in JRS, consistent with LAGG interfering more effectively in protein–free systems.

3.3.2. Long–range ordered (crystalline) starch structure

X–ray diffraction (XRD) analysis (Fig. 4) confirmed distinct crystalline patterns among the rice samples. JRF and JRS exhibited an A–type crystalline pattern, indicated by strong diffraction peaks at 15.2° and 23.1°, along with a partially resolved doublet at 17.5° and 18.2°. PRF and PRS displayed a C–type pattern—a mixture of A– and B–type features—with a notably lower DOC than their corresponding JR counterparts, indicating a weaker long–range crystalline order. The additional peak at 20.2° in PRF and PRS further implies the presence of

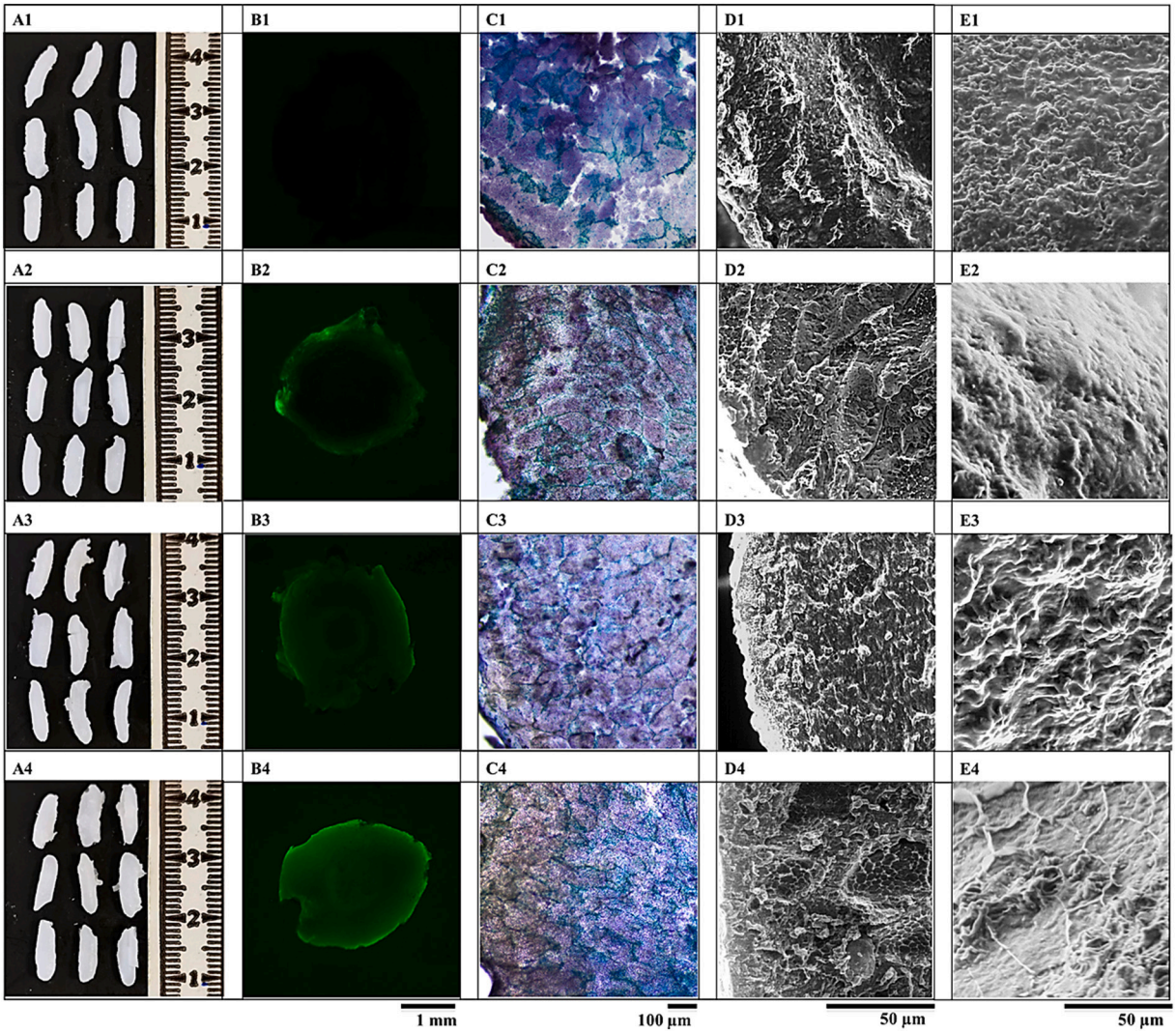

Fig. 5.1. Morphology of JR cooked with 0–3% LAGG. Images illustrating the samples containing different percentages of LAGG: (A) 0% LAGG, (B) 1% LAGG, (C) 2% LAGG, and (D) 3% LAGG. The columns represent visual inspection, fluorescence imaging, surface morphology, and microstructural analysis, respectively. Morphology of the whole cooked grain (scale bar: 1 cm) (A1–4); Fluorescence observation of cooked rice containing DTAF (5–(4,6–Dichlorotriazinyl) Aminofluorescein) labeled LAGG (scale bar: 1 mm) (B1–4). Microtone section of cooked grain viewed under light microscope (C1–4). Protein bodies appeared green with fast green staining, starch exhibited a blue–purple stain from Lugol's solution, amylopectin–rich regions were purple, and amylose–rich regions were blue (scale bar: 100 μm); cross–section (D1–4) and (E1–4) surface of cooked grain under ESEM (scale bar: 50 μm).

retrograded starch [58].

LAGG–treated samples showed a progressive reduction in DOC (Table 4), accompanied by shifts in diffraction intensity around 17.5° and 20.2°, features commonly associated with B– and V–type arrangements. These changes have previously been linked to amylose–hydrocolloid interactions, including the formation of amylose–LAGG complexes. The linear backbone and low–acyl substitution of LAGG are expected to facilitate close association with amylose single helices [59]. Specifically, the low–acyl structure of LAGG, with reduced steric hindrance compared to branched hydrocolloids and high–acyl gellan gum, allows its linear chains to closely associate with the hydrophilic exterior of amylose helices, primarily stabilizing the helical conformation through hydrogen bonding between hydroxyl groups and, potentially, weak hydrophobic interactions within the helical cavity [60]. Such interactions may promote the organization of amylose into V–type crystalline structures rather than re-formation of native A–type crystallinity.

Free LAGG also exhibits a diffraction peak near 20°, meaning that part of this signal likely arises from the hydrocolloid itself. White rice contains very low endogenous lipid (<0.5%), so amylose–lipid contributions cannot be fully excluded but are expected to be minor. Given these overlapping contributions, the diffraction peaks near 20° are conservatively interpreted as arising from the combined effects of LAGG presence, starch–hydrocolloid rearrangements, and minor native lipid interactions.

The presence of the protein matrix in rice grains (JR and PR) appeared to attenuate LAGG–induced reductions in starch crystallinity, with smaller DOC decreases compared with the corresponding starch isolates (JRS and PRS) (Table 4). This attenuation likely reflects spatial and interactional constraints imposed by the native protein–starch matrix rather than direct inhibition of LAGG functionality. In isolated starch, LAGG likely interferes with crystalline ordering by forming hydrogen bonds with hydroxyl groups, stabilizing the amorphous phase and impeding recrystallization [61].

3.3.3. Proximate composition and morphological properties of cooked rice types

As shown in Table 5, PR exhibited significantly higher protein and amylose contents compared to JR, despite similar total starch levels. SDS–PAGE analysis (Supplementary Fig. 3) confirmed rice–type differences in protein aggregation and thermal sensitivity, as previously

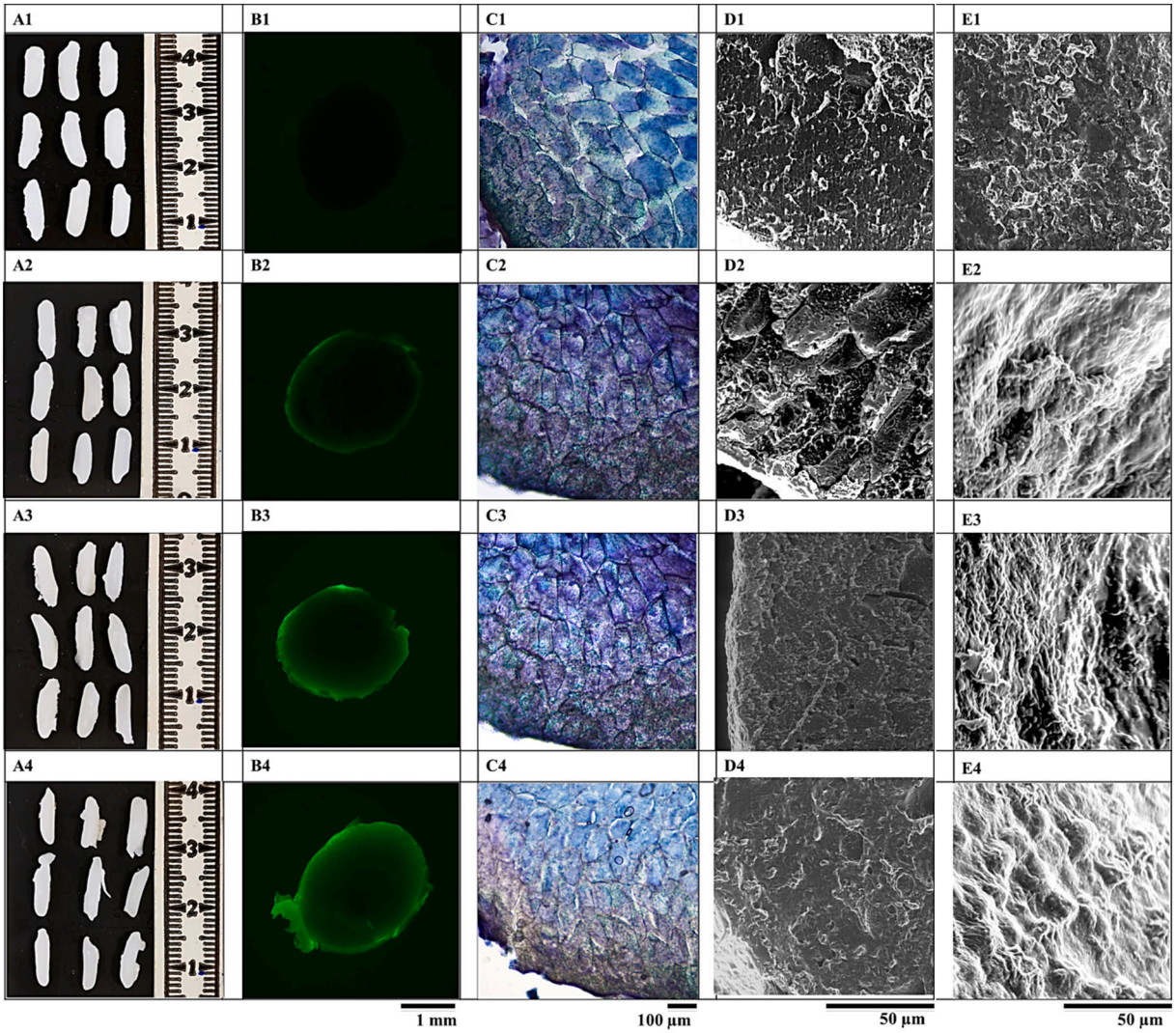

Fig. 5.2. Morphology of PR cooked with 0–3% LAGG. Images illustrating the samples containing different percentages of LAGG: (A) 0% LAGG, (B) 1% LAGG, (C) 2% LAGG, and (D) 3% LAGG. The columns represent visual inspection, fluorescence imaging, surface morphology, and microstructural analysis, respectively. Morphology of the whole cooked grain (scale bar: 1 cm) (A1–4); fluorescence observation of cooked rice containing DTAF (5–(4,6–Dichlorotriazinyl) Aminofluorescein) labeled LAGG (scale bar: 1 mm) (B1–4). Microtone section of cooked grain viewed under light microscope (C1–4). Protein bodies appeared green with fast green staining, starch exhibited a blue–purple stain from Lugol's solution, amylopectin–rich regions were purple, and amylose–rich regions were blue (scale bar: 100 μm); cross–section (D1–4) and (E1–4) surface of cooked grain under ESEM (scale bar: 50 μm).

discussed in the FTIR section. Under reducing conditions (Supplementary Fig. 3B), both rice types displayed typical glutelin and prolamin bands (15–57 kDa), with no evident dose–dependent changes following LAGG addition. Together with FTIR results (increased β–sheet content and reduced RC), suggest that LAGG modulates protein conformation primarily through non–covalent interactions and/or steric hindrance effects, likely stabilizing protein structures without altering disulfide bonding.

Morphological analysis revealed no significant differences in grain dimensions—length, width, thickness, sphericity, or surface area—between JR and PR, nor among LAGG–treated and untreated samples (Table 5, Figs. 5.1–5.2). These results indicate that LAGG incorporation, up to 3% (*w/w*), does not affect the external size or geometric parameters of cooked rice grains. However, at concentrations of 2–3%, the grain surface exhibits fabric–like string structures, which are likely attributable to the self–assembly properties of LAGG hydrogels [62]. In addition, microscopy uncovered distinct microstructural disparities between cooked JR and PR. PR showed a dense, continuous, green–stained matrix enveloping compact, purple–stained starch granules (Fig. 5.2C1). The green–stained regions, observed under light microscopy following Fast Green FCF staining, likely represent protein–rich domains, though non–protein components such as structural polysaccharides may also retain the dye [63]. This tightly organized matrix aligns with prior descriptions of cohesive starch–protein–cell wall domains in cereals such as brown rice and sorghum [64]. In contrast, JR exhibited a more fragmented matrix (Fig. 5.2C2), with discontinuous, green–stained regions and loosely arranged starch granules, suggesting inferior network formation and structural cohesion. ESEM corroborated these observations. JR displayed axial fissures, deformed granules, and a flaking outer layer, revealing disaggregated starch granules (Fig. 5.2D1, E1). Conversely, PR exhibited more cohesive fracture planes and fused granule agglomerates (Fig. 5.2D2, E2), indicative of enhanced internal bonding and structural integrity.

Although LAGG treatment did not significantly affect bulk morphometric properties, notable differences in internal microarchitecture emerged, particularly at higher LAGG concentrations (2–3%). Fluorescence microscopy revealed increased, green–stained intensity and surface localization at 1% LAGG (Figs. 5.1B and 5.2B), forming a discernible surface coating. At 2–3%, the stain penetrated deeper peripheral domains. Corresponding cross–sectional views of JR_1LAGG

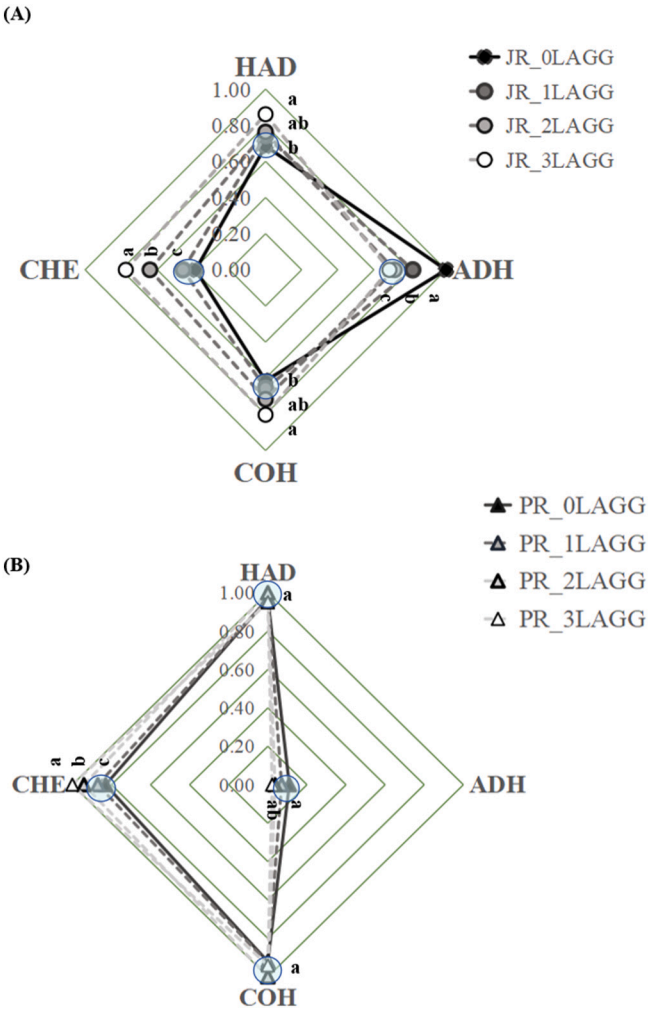

Fig. 6. Textural properties of JR (A) and PR (B) cooked in 0–3% (*w/w*) LAGG dispersions in water. Textural attributes including hardness (HAD), cohesiveness (COH), chewiness (CHE), and adhesiveness (ADH) were normalized on a parameter–specific basis. Each value represents the ratio of the sample measurement to the highest value recorded for that parameter (normalized to 1.00). Results are presented as mean ($n = 10$). Samples sharing the same letter and enclosed within the same statistical circle are not significantly different ($p > 0.05$).

and PR_1LAGG (Figs. 5.1C and 5.2C) revealed more cohesive matrix encapsulation of starch granules compared to untreated controls, which showed disrupted organization and diffuse starch domains. At elevated LAGG concentrations (2–3%), structural disintegration became apparent. The protein–starch matrix showed fragmentation, with reduced granule packing and the emergence of filamentous gel structures (Figs. 5.1D and 5.2D). These observations align with the fabric–-like structures seen at grain surface, suggesting that while lower concentrations may reinforce matrix stability, excessive inclusion can disrupt starch–protein interactions. This concentration–dependent structural modulation implies potential applications in tailoring rice texture and digestibility via controlled hydrocolloid incorporation.

3.4. Textural profile

The radar plots (Fig. 6) summarize the instrumental textural properties of JR and PR cooked with 0–3% LAGG. Without LAGG, PR exhibited greater hardness, chewiness, and lower adhesiveness than JR, consistent with its inherently firmer texture, as reported in previous studies [65,66]. LAGG incorporation progressively increased JR hardness and chewiness while reducing adhesiveness. Significant changes occurred only at ≥2%, while 1% LAGG did not differ from the control ($p > 0.05$). These effects align with microstructural observations showing surface hydrogel formation at 1% and a denser interfacial network at 2–3% (Fig. 5.1), which likely restricted water mobility, starch swelling and amylose leaching [67,68], and reinforced the protein–starch matrix [69]. PR showed minimal changes in texture, with only a slight increase in chewiness, likely due to its pre–existing structured protein–starch matrix, which was less affected by LAGG treatment. Overall, the observed instrumental texture values remained within ranges reported for conventionally cooked long–grain rice, suggesting that LAGG incorporation up to 3% does not induce extreme textural deviation. While texture profile analysis provides objective parameters related to sensory perception, formal sensory evaluation would be required to directly assess consumer acceptability.

3.4.1. *In–vitro starch digestibility of post–textual analysis samples*

The in–vitro digestibility of starch and protein in JR and PR—treated with varying concentrations of LAGG—was assessed post–TPA using in–vitro enzymatic hydrolysis coupled with kinetic models (Fig. 7). While TPA is not a direct simulation of oral processing, it provides insight into how textural properties influence the structural integrity of rice matrices and their susceptibility to enzymatic breakdown during digestion [70,71].

Starch digestograms followed a biphasic kinetic pattern (Table 6), characterized by an initial rapid phase, observed within the initial 20 min, followed by a gradual progression toward a plateau ($k_1 > k_2$). This reflects heterogeneous accessibility of starch fractions—characterized by an initial rapid hydrolysis of accessible starch, followed by a slower phase involving enzyme–resistant or structurally constrained starch fractions. JR demonstrated significantly higher starch digestibility than parboiled rice (PR), with a faster rate (k_1 = 0.096 min^{-1} vs. 0.061 min^{-1}), greater initial hydrolysis ($C_0 = 7.31 \pm 1.46\%$ vs. $3.87 \pm 0.28\%$), and higher final extent at 180 min ($84.62 \pm 2.13\%$ vs. $73.77 \pm 1.86\%$, Fig. 7C, D). JR also had a greater proportion of rapidly digestible starch (RDS = $67.40 \pm 1.15\%$) and a higher predicted glycemic index (pGI = 81.6 ± 2.0) compared to PR (RDS = $41.84 \pm 1.93\%$, pGI = 66.1 ± 2.5). These findings support the classification of JR as a high–GI food (>70), while PR remains in the moderate–GI (55-70) range [72].

LAGG addition progressively reduced C_0, k_1, and $C_{1\infty}$, while increasing $C_{2\infty}$, particularly in JR. For example, in JR samples C_0, decreased from 7.31% (JR_0LAGG) to 2.85% (JR_3LAGG), k_1 declined from 0.096 to 0.057 min^{-1}, $C_{1\infty}$ dropped from 66.70% to 47.18%. Concurrently, the slowly digestible fraction ($C_{2\infty}$) increased substantially—from 25.70% to 49.98% —indicating a shift in the digestogram profile toward a larger slowly digestible fraction, particularly in JR. Consistent with this shift, the transition time (t_{int}) was increased from 19 to 21 min, and digestibility at transition (C_{int}) declined from 62.56% to 35.44% with increasing LAGG levels. These trends suggest that LAGG addition may reduce enzymatic hydrolysis of starch by potentially promoting the formation of a denser, more cohesive matrix and reduced porosity. This interpretation is consistent with the microstructural observations (Fig. 5.1–5.2) and textural changes (Fig. 6). Post-TPA particle size (d_{50}; median fragment diameter) increased (Table 6; e.g., JR_3LAGG = 1.23 ± 0.01 mm vs. JR_0LAGG = 1.16 ± 0.01 mm). These larger fragments may also lower surface area–to–volume ratios, limiting enzyme diffusion and delaying digestion onset. Similar but less pronounced effects were observed in PR, where C_0 decreased from 3.87% (PR_0LAGG) to 2.18% (PR_3LAGG), k_1 from 0.061 to 0.050 min^{-1}, and $C_{1\infty}$ from 54.76% to 49.06%, while $C_{2\infty}$ increased from 41.37% to 48.76%.

Protein digestion followed a single–phase first–order kinetic model ($R^2 > 0.90$, Table 7), with no inflection points observed in LoS analysis, indicating uniform hydrolysis kinetics. This likely reflects the more homogeneous distribution and structural accessibility of proteins in the cooked rice matrix compared with starch's granular and hierarchical

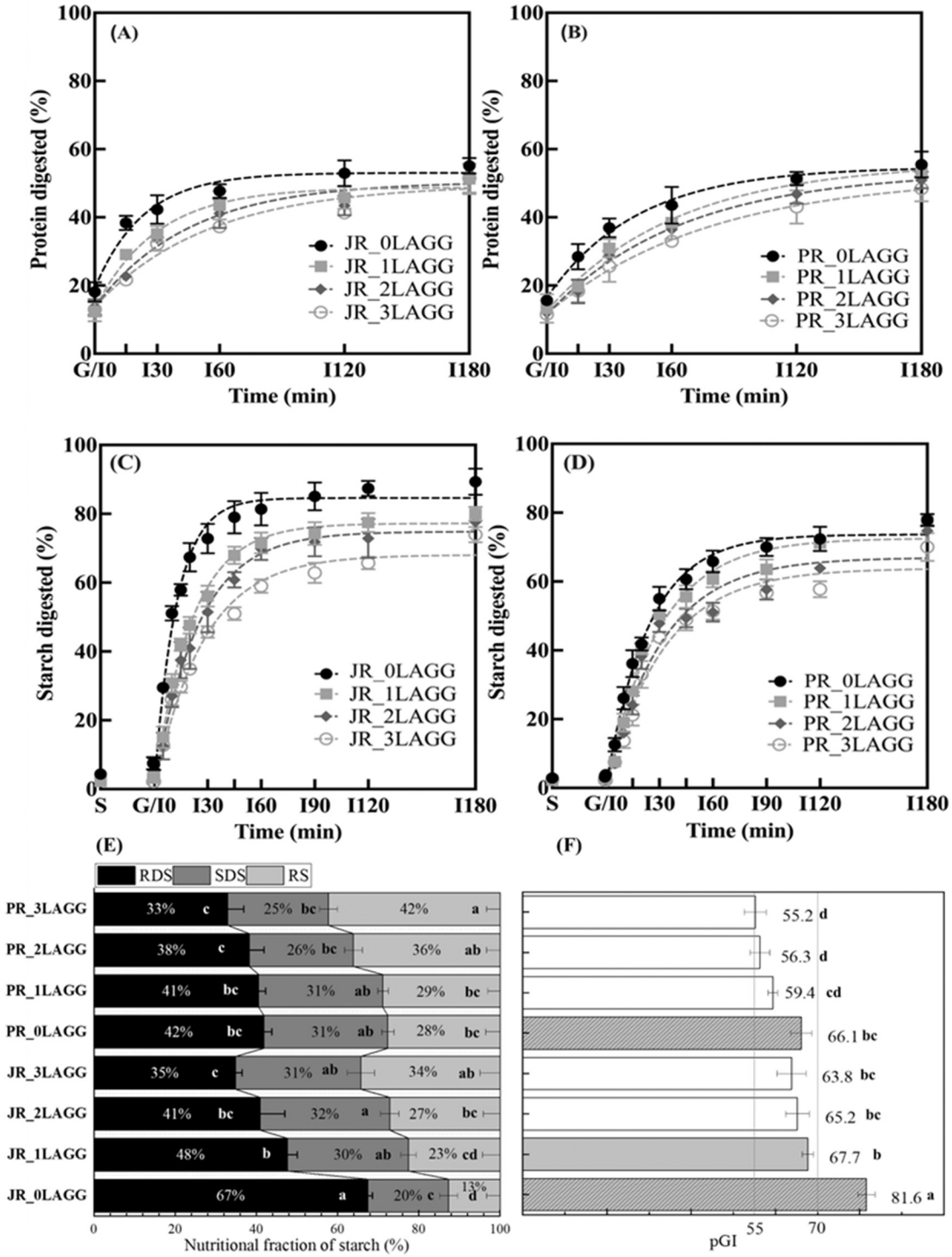

Fig. 7. In–vitro protein and starch digestibility, starch fractions, and predicted glycemic index (pGI) of cooked rice samples treated with 0–3% LAGG. (A, B) Protein digested (%) is over 180 min for JR and PR samples. (C, D) Starch digested (%) over 180 min for JR and PR samples. Digested (%) denotes hydrolysis extent (starch: reducing sugars; protein: free amino groups) (E) Nutritional starch fractions: rapidly digestible starch (RDS), slowly digestible starch (SDS), and resistant starch (RS). (F) pGI. Data represents mean ± SD ($n = 4$). Samples sharing the same letter within each panel (vertical comparison) are not significantly different ($p > 0.05$).

structure. Protein hydrolysis by pepsin and trypsin—targeting specific residues (pepsin: hydrophobic/aromatic; trypsin: basic)—may also be less dependent on matrix swelling or enzyme diffusion.

JR exhibited higher protein digestibility than PR, reflected in greater initial hydrolysis ($Y_0 = 19.2\%$) and hydrolysis rate ($k = 0.043\ min^{-1}$) than PR_0LAGG ($Y_0 = 16.4\%$; $k = 0.028\ min^{-1}$). It is likely due to fewer heat–induced aggregates and more exposed cleavage sites. In PR, parboiling promotes protein–starch interactions and aggregation, which can shield pepsin– (Phe, Leu) and trypsin–specific (Lys, Arg) peptide bonds from enzymatic access [73]. LAGG addition likely reduced protein digestibility parameters (Y_0, k, and Y_∞) by reinforcing a denser, acid–stable matrix that limited pepsin access during gastric digestion. Final digestibility remained moderate (48–56%) as gel relaxation at intestinal pH allowed trypsin access to protein substrates.

Table 6
Kinetic parameters of in–vitro starch digestion of cooked rice with 0–3% LAGG.

	d_{50} (mm)	C_0 (%)	k_1 (min^{-1})	$C_{1\infty}$ (%)	k_2 (min^{-1})	$C_{2\infty}$ (%)	t_{int} (min)	C_{int} (%)	R^2
JR_0LAGG	1.16 ± 0.01 ^{c}	7.31 ± 1.46 ^{a}	0.096 ± 0.003 ^{a}	66.70 ± 3.51 ^{a}	0.016 ± 0.002 ^{c}	25.70 ± 2.13 ^{c}	19 ± 1 ^{bc}	62.56 ± 3.31 ^{a}	0.9494
JR_1LAGG	1.22 ± 0.01 ^{bc}	3.18 ± 0.51 ^{b}	0.067 ± 0.003 ^{b}	59.78 ± 2.23 ^{b}	0.030 ± 0.002 ^{a}	36.41 ± 4.02 ^{b}	25 ± 3 ^{ab}	51.86 ± 5.09 ^{b}	0.9047
JR_2LAGG	1.22 ± 0.02 ^{bc}	2.84 ± 0.51 ^{b}	0.062 ± 0.004 ^{b}	54.45 ± 3.11 ^{b}	0.030 ± 0.004 ^{a}	42.71 ± 3.54 ^{b}	16 ± 1 ^{c}	37.63 ± 3.87 ^{c}	0.9484
JR_3LAGG	1.23 ± 0.01 ^{b}	2.85 ± 0.55 ^{b}	0.057 ± 0.003 ^{bc}	47.18 ± 1.56 ^{c}	0.020 ± 0.003 ^{bc}	49.98 ± 0.52 ^{a}	21 ± 2 ^{bc}	35.44 ± 2.30 ^{c}	0.9304
PR_0LAGG	1.29 ± 0.01 ^{a}	3.87 ± 0.28 ^{b}	0.061 ± 0.003 ^{b}	54.76 ± 3.32 ^{b}	0.022 ± 0.002 ^{b}	41.37 ± 3.25 ^{b}	25 ± 2 ^{ab}	46.26 ± 3.32 ^{b}	0.9447
PR_1LAGG	1.30 ± 0.01 ^{a}	2.81 ± 0.51 ^{b}	0.052 ± 0.002 ^{c}	57.59 ± 1.46 ^{b}	0.020 ± 0.002 ^{b}	39.60 ± 1.83 ^{b}	28 ± 1 ^{a}	46.65 ± 1.92 ^{b}	0.9479
PR_2LAGG	1.28 ± 0.01 ^{a}	3.17 ± 0.29 ^{b}	0.056 ± 0.002 ^{b}	58.05 ± 1.44 ^{b}	0.025 ± 0.001 ^{b}	38.78 ± 1.65 ^{b}	26 ± 1 ^{ab}	47.48 ± 2.76 ^{b}	0.9426
PR_3LAGG	1.30 ± 0.02 ^{a}	2.18 ± 0.64 ^{b}	0.050 ± 0.002 ^{c}	49.06 ± 2.24 ^{c}	0.018 ± 0.003 ^{c}	48.76 ± 3.22 ^{a}	28 ± 2 ^{a}	39.03 ± 3.36 ^{c}	0.9051

Values are means ± standard deviation. Within each column, values denoted by the same letter are not significantly different ($p > 0.05$). 1LAGG, 2LAGG and 3LAGG indicated the cooked JR and PR with 1, 2 and 3 g LAGG per 100 g rice, respectively. d_{50} is the median particle size after TPA tests; Co is initial digested starch percentage at the beginning of intestinal phase; k_1 and k_2 arethe apparent first-order rate constants (min^{-1}) for the rapid and slow phases, respectively; $C_{1\infty}$ and $C_{2\infty}$the expected digestion extent (%)for the rapid and slow phases, respectively. t_{int} is the transition time (min) between phases, and C_{int} is the digested starch (%) at t_{int}. R^2 is the coefficient of determination for the model fit.

Table 7
First–order kinetic parameters for in–vitro protein digestion of JR and PR rice samples treated with 0–3% LAGG.

	Y_0 (%)	k (min^{-1})	Y_∞ (%)	*Span* (%)	R^2
JR_0LAGG	19.16 ± 1.96 ^{a}	0.043 ± 0.007 ^{a}	53.07 ± 1.38 ^{b}	33.91 ± 2.29 ^{b}	0.9360
JR_1LAGG	13.11 ± 1.90 ^{b}	0.034 ± 0.005 ^{b}	48.77 ± 1.48 ^{c}	35.66 ± 2.26 ^{b}	0.9434
JR_2LAGG	13.74 ± 1.85 ^{b}	0.022 ± 0.004 ^{c}	50.50 ± 2.00 ^{bc}	36.76 ± 2.39 ^{b}	0.9430
JR_3LAGG	13.75 ± 3.32 ^{b}	0.018 ± 0.007 ^{c}	49.69 ± 4.44 ^{bc}	35.93 ± 4.72 ^{b}	0.9576
PR_0LAGG	16.41 ± 1.76 ^{ab}	0.028 ± 0.004 ^{b}	55.80 ± 1.82 ^{a}	39.39 ± 2.24 ^{ab}	0.9531
PR_1LAGG	11.51 ± 1.56 ^{b}	0.016 ± 0.003 ^{d}	55.16 ± 2.52 ^{a}	43.65 ± 2.48 ^{a}	0.9656
PR_2LAGG	11.47 ± 1.21 ^{b}	0.015 ± 0.002 ^{d}	53.50 ± 2.05 ^{ab}	42.03 ± 1.99 ^{a}	0.9771
PR_3LAGG	11.67 ± 0.64 ^{b}	0.013 ± 0.004 ^{d}	52.10 ± 1.45 ^{b}	40.43 ± 1.33 ^{a}	0.9844

Values are means ± standard deviation. Within each column, values denoted by the same letter are not significantly different ($p > 0.05$).0LAGG, 1LAGG, 2LAGG and 3LAGG indicated the cooked JR and PR with 0, 1, 2 and 3 g LAGG per 100 g rice, respectively. Y_0: initial hydrolysis (%), k_1: rate constant (min^{-1}), Y_∞: final extent of hydrolysis (%), *Span*: difference between Y_∞ and Y_0.

LAGG addition modulated the digestibility profiles of both starch and protein, notably shifting starch digestion toward a slower, more sustained pattern—particularly in JR. These changes were associated with increased resistant starch (RS; 12.63% to 34.26%) and reduced predicted glycemic index (pGI; 81.6 to 63.8). PR exhibited a similar, though less pronounced, trend, with RS increasing from 27.62% to 42.26% and pGI decreasing from 66.1 to 55.2. Notably, PR_3LAGG showed the highest RS content (42.26 ± 3.36%) and the lowest pGI (55.2 ± 2.6), highlighting the potential of LAGG for developing functional rice products for glycemic management.

3.5. Discussion: multivariate analysis of factors influencing PGI of rice

PCA (Fig. 8) explained 91.4% of the total variance in pGI, with PC1 (69.23%) and PC2 (26.28%) capturing key structural and digestive contributors (Fig. 8). Variables loading positively on PC1—including β–sheet content, post–compression particle size (d_{50}), chewiness, RS, and LAGG incorporation—were associated with slower starch digestion and lower pGI values, indicating a close association between LAGG–related structural attributes and reduced pGI.

These observations can be interpreted within a hierarchical structure–function framework. At the molecular level, LAGG addition was associated with modest increases in β–sheet content without substantial shifts in amide I peak positions, consistent with previous reports that gellan gum does not fundamentally alter protein secondary structure but

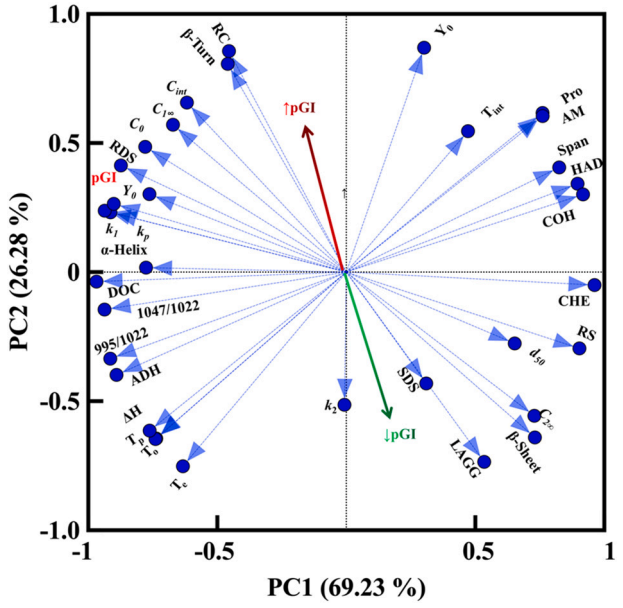

Fig. 8. Principal components analysis: loading plot of PCs illustrating relationships among physicochemical, structural, textural, and digestive properties of TPA–tested rice samples. RDS, rapidly digestible starch; SDS, slowly digestible starch; RS, resistant starch; pGI, predicted glycemic index; T_o: onset temperature; T_p: peak temperature; T_e: end temperature; ΔH_{en} is the enthalpy of gelatinization; protein digestibility parameters (Y_0, k_p, Y_∞, and *Span*); AM: amylose content; Pro: protein content; starch digestibility parameters of rapid (C_0, k_1, $C_{1\infty}$) slow (k_2, $C_{2\infty}$) phases and intersect–phase point (T_{int}, C_{int}); Textural profile parameters includes hardness (HAD), cohesiveness (COH), chewiness (CHE), and adhesiveness (ADH); and median particle size after TPA compression (d_{50})

may stabilize ordered conformations through hydrogen bonding and steric effects [74]. At the meso–structural level, microscopy revealed semi–translucent, LAGG–enriched interfacial coatings and a denser protein–starch–LAGG matrix. This compact architecture is likely to act as a diffusion barrier, limiting enzyme penetration and slowing both starch and protein hydrolysis. At the macro–structural scale, LAGG incorporation was associated with increased hardness, chewiness, and d_{50}, particularly in JR. These effects were concentration–dependent: 1% LAGG produced no significant textural changes relative to the control, while ≥2% resulted in moderate increases that remained within ranges comparable to PR hardness, alongside elevated SDS and RS levels. In contrast, untreated controls exhibited a more disrupted matrix structure and greater enzymatic accessibility, consistent with higher pGI values.

PC2 differentiated samples primarily by digestion kinetics. Higher gastric protein hydrolysis (Y_0), faster proteolysis (k_p), and accelerated

starch digestion during the rapid phase (k_1, $C_{1\infty}$), together with higher RDS, were aligned with increased α–helix and RC content. This association suggests that protein conformations more susceptible to proteolysis may weaken matrix integrity during digestion, indirectly enhancing starch accessibility and contributing to higher pGI. The observed alignment between higher protein digestibility parameters (Y_0, Y_∞) and elevated RDS and starch hydrolysis metrics (C_0, $C_{1\infty}$) underscores the interdependence of protein and starch breakdown. LAGG–treated samples, by contrast, retained more resistant protein conformations, which may have contributed to preserving matrix integrity and concurrently limiting both protein and starch digestibility.

In addition to protein conformation and structural–mechanical attributes (e.g., chewiness and d_{50}), compositional factors (protein and amylose content), and thermal properties (T_0, T_p, Tc, and ΔH_{en}), exert dual roles in modulating pGI. Their positive association with PC1 suggests a contribution to digestion resistance, likely through enhanced protein barriers and amylose–driven resistant starch formation [47]. Meanwhile, their alignment with PC2 may reflect conditions under which these advantages are lost during cooking or digestion, as reported previously [75].

Overall, the PCA results suggest that pGI modulation arises from coordinated effects across molecular, *meso*–, and macro–structural scales rather than from a single dominant parameter. From an application perspective, variables associated with reduced pGI clustered consistently at LAGG concentration levels of 1–3%, suggesting that this range enables sufficient matrix reinforcement to slow enzymatic hydrolysis without major disruption to grain integrity or instrumental texture. This balance between digestion resistance and texture preservation underscores the practical relevance of the optimal formulation window identified in this study.

In terms of industrial feasibility, the low concentration levels (1–3%) are advantageous as they minimize ingredient loading and avoid excessive viscosity increases that could compromise mixing, hydration, or uniform cooking. Concentrations above 3% could lead to practical limitations during cooking, including reduced rice immersion and less uniform gelatinization, which informed the upper boundary of the formulation range evaluated. Importantly, LAGG can be applied as a pre–hydrated dispersion in the cooking medium, which is compatible with existing wet–processing practices and does not require modification of the rice grain or specialized equipment. While sensory evaluation and cost analysis were beyond the scope of this study, the moderate use levels and preserved textural properties suggest a formulation strategy that is technically implementable and compatible with consumer–relevant quality attributes.

4. Conclusions

This study demonstrated that incorporating low–acyl gellan gum (LAGG) during rice cooking modifies the protein–starch matrix and reduces enzymatic starch digestibility while maintaining acceptable textural properties, thereby supporting the study hypothesis. LAGG reduced starch digestibility through multi–scale structural effects, including interfacial hydrogel coating, suppression of starch recrystallization, and stabilization of protein–starch networks, leading to lower rapidly digestible starch fractions and reduced predicted glycemic index—particularly in jasmine rice—while only moderate and acceptable textural changes were observed within a practical formulation range (1–3% *w/w*).

While this study focused on freshly cooked rice systems, the stability of LAGG–induced structural modifications during storage, reheating, and application in complex food formats (e.g., ready–to–eat rice or set meals) remains to be established. Future studies incorporating sensory evaluation and shelf–life assessment will be essential to support translation into commercial products. Overall, these findings highlight LAGG as a promising hydrocolloid for glycemic modulation via interfacial matrix engineering without major disruption to processing or texture.

CRediT authorship contribution statement

Qingsu Liu: Writing – original draft, Visualization, Methodology, Investigation, Formal analysis, Data curation, Conceptualization. **Vincenzo Di Bari:** Writing – review & editing, Validation, Supervision, Project administration, Conceptualization. **Nicholas James Watson:** Writing – review & editing, Supervision, Resources, Project administration, Conceptualization.

Declaration of Generative AI and AI-assisted technologies in the writing process

Generative AI was used in the manuscript for improving language and readability.

Declaration of competing interest

The authors declare that they have no known competing financial interests or personal relationships that could have appeared to influence the work reported in this paper.

Acknowledgements

Thanks to the University of Nottingham for providing funding for this work.

Appendix A. Supplementary data

Supplementary data to this article can be found online at https://doi.org/10.1016/j.ijbiomac.2026.150373.

Data availability

Data will be made available on request.

References

[1] L. Yu, M.S. Turner, M. Fitzgerald, J.R. Stokes, T. Witt, Review of the effects of different processing technologies on cooked and convenience rice quality, Trends Food Sci. Technol. 59 (2017) 124–138, https://doi.org/10.1016/J.TIFS.2016.11.009.

[2] F.S. Atkinson, J.C. Brand-Miller, K. Foster-Powell, A.E. Buyken, J. Goletzke, International tables of glycemic index and glycemic load values 2021: a systematic review, Am. J. Clin. Nutr. 114 (5) (2021) 1625–1632, https://doi.org/10.1093/AJCN/NQAB233.

[3] N. Ikeda, M. Yamaguchi, N. Nishi, Health and economic impacts of increased brown rice consumption on type 2 diabetes in Japan: a simulation study, 2019–2029, Nutrients 17 (3) (2025) 532, https://doi.org/10.3390/NU17030532/S1.

[4] H. Yusri, S.J.L. Ou, D. Yang, M. Ting, W.L. Liew, S.A. Rebello, et al., Acceptance and feasibility of novel staple foods among individuals with type 2 diabetes in Singapore: a mixed methods study, Front. Nutr. 12 (2025) 1594890, https://doi.org/10.3389/FNUT.2025.1594890/BIBTEX.

[5] P.O. Suklaew, C. Chusak, S. Adisakwattana, Physicochemical and functional characteristics of rd43 rice flour and its food application, Foods 9 (12) (2020), https://doi.org/10.3390/foods9121912.

[6] C. Cai, Y. Tian, Z. Yu, C. Sun, Z. Jin, In vitro digestibility and predicted glycemic index of chemically modified rice starch by one–step reactive extrusion, Starch – Stärke 72 (1–2) (2020) 1900012, https://doi.org/10.1002/STAR.201900012.

[7] D. Cabral, A.P. Moura, S.C. Fonseca, J.C. Oliveira, L.M. Cunha, Exploring rice consumption habits and determinants of choice, aiming for the development and promotion of rice products with a low glycaemic index, Foods 13 (2) (2024) 301, https://doi.org/10.3390/FOODS13020301/S1.

[8] Z. Zhao, Z. Wang, J. Zhu, A. Xu, D.J. McClements, J. Chen, et al., How differences in rice texture and oral physiology affect sensory preference and eating behavior of consumers: a generalized additive models (GAMs) approach, Food Struct. 44 (2025) 100418, https://doi.org/10.1016/J.FOOSTR.2025.100418.

[9] A.K. Jukanti, P.A. Pautong, Q. Liu, N. Sreenivasulu, Low glycemic index rice—a desired trait in starchy staples, Trends Food Sci. Technol. 106 (2020) 132–149, https://doi.org/10.1016/J.TIFS.2020.10.006.

[10] M. Ma, Z. Gu, L. Cheng, Z. Li, C. Li, Y. Hong, Effect of hydrocolloids on starch digestion: a review, Food Chem. 444 (2024) 138636, https://doi.org/10.1016/J.FOODCHEM.2024.138636.

[11] S. Blanquet-Diot, O. François, S. Denis, M. Hennequin, M.A. Peyron, Importance of oral phase in in vitro starch digestibility related to wholegrain versus refined pastas

and mastication impairment, Food Hydrocoll. 112 (2021) 106277, https://doi.org/10.1016/j.foodhyd.2020.106277.
[12] K.M. Kanyuck, T.B. Mills, I.T. Norton, A.B. Norton-Welch, Release of glucose and maltodextrin DE 2 from gellan gum gels and the impacts of gel structure, Food Hydrocoll. 122 (2022) 107090, https://doi.org/10.1016/J.FOODHYD.2021.107090.
[13] J.F. Bradbeer, R. Hancocks, F. Spyropoulos, I.T. Norton, Low acyl gellan gum fluid gel formation and their subsequent response with acid to impact on satiety, Food Hydrocoll. 43 (2015) 501–509, https://doi.org/10.1016/j.foodhyd.2014.07.006.
[14] P.C. Wanniarachchi, Iranga, T. Paranagama, Piyumi, A. Idangodage, B. Nallaperuma, et al., Natural polymer–based hydrogels: types, functionality, food applications, environmental significance and future perspectives: an updated review, Food Biomacromol. 2 (1) (2025) 84–105, https://doi.org/10.1002/FOB2.70000.
[15] Hussain S.M. Lalarukh, S. Ali, E. Yilmaz, A.F. Zahoor, A. Javid, et al., Microencapsulation: an innovative technology in modern science, Polym. Adv. Technol. 36 (1) (2025) e70066, https://doi.org/10.1002/PAT.70066. PAGEGROUP:STRING:PUBLICATION.
[16] D.V. Ranawana, C.J.K. Henry, H.J. Lightowler, D. Wang, Glycaemic index of some commercially available rice and rice products in Great Britain, Int. J. Food Sci. Nutr. 60 (Suppl. 4) (2009) 99–110, https://doi.org/10.1080/09637480802516191.
[17] M.A. Fitzgerald, S. Rahman, A.P. Resurreccion, J. Concepcion, V.D. Daygon, S. S. Dipti, et al., Identification of a major genetic determinant of glycaemic index in rice, Rice 4 (2) (2011) 66–74, https://doi.org/10.1007/S12284–011–9073–Z.
[18] A. Brodkorb, L. Egger, M. Alminger, P. Alvito, R. Assunção, S. Ballance, et al., INFOGEST static in vitro simulation of gastrointestinal food digestion, Nat. Protoc. 14 (4) (2019) 991–1014, https://doi.org/10.1038/s41596–018–0119–1.
[19] Singh Sodhi, N. Singh, Morphological, thermal and rheological properties of starches separated from rice cultivars grown in India, Food Chem. 80 (1) (2003) 99–108, https://doi.org/10.1016/S0308–8146(02)00246–7.
[20] L. Zhu, G. Wu, L. Cheng, H. Zhang, L. Wang, H. Qian, et al., Effect of soaking and cooking on structure formation of cooked rice through thermal properties, dynamic viscoelasticity, and enzyme activity, Food Chem. 289 (2019) 616–624, https://doi.org/10.1016/j.foodchem.2019.03.082.
[21] D.E. Garcia-Valle, L.A. Bello-Pérez, E. Agama-Acevedo, J. Alvarez-Ramirez, Effects of mixing, sheeting, and cooking on the starch, protein, and water structures of durum wheat semolina and chickpea flour pasta, Food Chem. 360 (2021) 129993, https://doi.org/10.1016/J.FOODCHEM.2021.129993.
[22] A. Fetouhi, L. Benatallah, A. Nawrocka, M. Szymańska-Chargot, A. Bouasla, M. Tomczyńska-Mleko, et al., Investigation of viscoelastic behaviour of rice–field bean gluten–free dough using the biophysical characterization of proteins and starch: a FT–IR study, J. Food Sci. Technol. 56 (3) (2019) 1316–1327, https://doi.org/10.1007/s13197–019–03602–2.
[23] W. Al-Ansi, B.M. Sajid, Mahdi Aa, Q.A. Al-Maqtari, A. Al-Adeeb, A. Ahmed, et al., Molecular structure, morphological, and physicochemical properties of highlands barley starch as affected by natural fermentation, Food Chem. 356 (2021) 129665, https://doi.org/10.1016/J.FOODCHEM.2021.129665.
[24] H.W. Choi, H.S. Kim, Hydroxypropylation and acetylation of rice starch: effects of starch protein content, Food Sci. Biotechnol. 31 (9) (2022) 1169, https://doi.org/10.1007/S10068–022–01106–Y.
[25] I. Chakraborty, S. Pallen, Y. Shetty, N. Roy, N. Mazumder, Advanced microscopy techniques for revealing molecular structure of starch granules, Biophys. Rev. 12 (1) (2020) 105–122, https://doi.org/10.1007/S12551–020–00614–7.
[26] W.Y. Chiou, K. Tsugane, T. Kawamoto, M. Maekawa, Easy sectioning of whole grain of rice using cryomicrotome, Breed. Sci. 68 (3) (2018) 381, https://doi.org/10.1270/JSBBS.17103.
[27] M.N. Khin, S. Ahammed, F. Zhong, Development of (5–(4,6–dichlorotriazinyl) aminofluorescein) DTAF–labelled polysaccharides for characterization of microstructure and phase distribution of composite hydrogel visualization of hydrogels using CLSM, Food Biosci. (2021) 41, https://doi.org/10.1016/j.fbio.2021.100909.
[28] J. Dang, L. Copeland, Studies of the fracture surface of rice grains using environmental scanning electron microscopy, J. Sci. Food Agric. 84 (2004) 707–713, https://doi.org/10.1002/jsfa.1671.
[29] M. Boluda-Aguilar, A. Taboada-Rodríguez, A. López-Gómez, F. Marín-Iniesta, G. V. Barbosa-Cánovas, Quick cooking rice by high hydrostatic pressure processing, LWT Food Sci. Technol. 51 (1) (2013) 196–204, https://doi.org/10.1016/j.lwt.2012.09.021.
[30] J.M. Fernandes, D.A. Madalena, A.C. Pinheiro, A.A. Vicente, Rice in vitro digestion: application of INFOGEST harmonized protocol for glycemic index determination and starch morphological study, J. Food Sci. Technol. 57 (4) (2020) 1393, https://doi.org/10.1007/S13197–019–04174–X.
[31] M. Lever, A new reaction for colorimetric determination of carbohydrates, Anal. Biochem. 47 (1) (1972) 273–279, https://doi.org/10.1016/0003–2697(72)90301–6.
[32] H. Xu, J. Zhou, J. Yu, S. Wang, L. Copeland, S. Wang, Revealing the mechanisms of starch amylolysis affected by tea catechins using surface plasmon resonance, Int. J. Biol. Macromol. 145 (2020) 527–534, https://doi.org/10.1016/J.IJBIOMAC.2019.12.161.
[33] L. Jiménez-Munoz, A. Brodkorb, L.G. Gómez-Mascaraque, M. Corredig, Effect of heat treatment on the digestion behavior of pea and rice protein dispersions and their blends, studied using the semi–dynamic INFOGEST digestion method, Food Funct. 12 (18) (2021) 8747–8759, https://doi.org/10.1039/d1fo01223a.
[34] A. Rieder, N.K. Afseth, U. Böcker, S.H. Knutsen, B. Kirkhus, H.K. Mæhre, et al., Improved estimation of in vitro protein digestibility of different foods using size exclusion chromatography, Food Chem. 358 (2021) 129830, https://doi.org/10.1016/J.FOODCHEM.2021.129830.
[35] C.H. Edwards, M. Maillot, R. Parker, F.J. Warren, A comparison of the kinetics of in vitro starch digestion in smooth and wrinkled peas by porcine pancreatic alpha–amylase, Food Chem. 2018 (244) (June 2017) 386–393, https://doi.org/10.1016/j.foodchem.2017.10.042.
[36] Z. Wang, G. Chen, X. Chen, Q. Xia, Y. Yin, N. Xiao, et al., Molecular mechanism of Golden Pomfret myofibrillar protein digestion inhibition by malondialdehyde–mediated oxidation based on peptidomics analysis, Food Chem. X 29 (2025) 102713, https://doi.org/10.1016/J.FOCHX.2025.102713.
[37] I. Goñi, A. Garcia-Alonso, F. Saura-Calixto, A starch hydrolysis procedure to estimate glycemic index, Nutr. Res. 17 (3) (1997) 427–437, https://doi.org/10.1016/S0271–5317(97)00010–9.
[38] S. Puncha-Arnon, D. Uttapap, Rice starch vs. rice flour: differences in their properties when modified by heat–moisture treatment, Carbohydr. Polym. 91 (1) (2013) 85–91, https://doi.org/10.1016/j.carbpol.2012.08.006.
[39] S. Sittipod, Y.C. Shi, Changes in physicochemical properties of rice starch during steeping in the parboiling process, J. Cereal Sci. 69 (2016) 398–405, https://doi.org/10.1016/J.JCS.2016.05.010.
[40] E.H. Jang, S.J. Lee, J.Y. Hong, H.J. Chung, Y.T. Lee, B.S. Kang, et al., Correlation between physicochemical properties of japonica and indica rice starches, LWT Food Sci. Technol. 66 (2016) 530–537, https://doi.org/10.1016/J.LWT.2015.11.001.
[41] X. Lu, R. Ma, H. Qiu, C. Sun, Y. Tian, Mechanism of effect of endogenous/exogenous rice protein and its hydrolysates on rice starch digestibility, Int. J. Biol. Macromol. 193 (2021) 311–318, https://doi.org/10.1016/J.IJBIOMAC.2021.10.140.
[42] A. Bruna, T.P. Ricardo, B. Josiane, A.S. Rafael, C.E. Moacir, R.Z. Elessandra, R.G. D. Alvaro, The effects of heat–moisture treatment of rice grains before parboiling on viscosity profile and physicochemical properties, Int. J. Food Sci. Technol. 49 (8) (August 2014) 1939–1945, https://doi.org/10.1111/ijfs.12580.
[43] M.R. Islam, N. Shimizu, T. Kimura, Effect of processing conditions on thermal properties of parboiled rice, Food Sci. Technol. Res. 8 (2) (2002) 131–136, https://doi.org/10.3136/FSTR.8.131.
[44] C. Chi, X. Li, Y. Zhang, L. Chen, F. Xie, L. Li, et al., Modulating the in vitro digestibility and predicted glycemic index of rice starch gels by complexation with gallic acid, Food Hydrocoll. 89 (2019) 821–828, https://doi.org/10.1016/J.FOODHYD.2018.11.016.
[45] G. Sworn, L. Stouby, Gellan gum, in: Handbook of Hydrocolloids, 2021, pp. 855–885, https://doi.org/10.1016/B978–0–12–820104–6.00009–7.
[46] R. Cai, B. Klamczynska, B.K. Baik, Preparation of bean curds from protein fractions of six legumes, J. Agric. Food Chem. 49 (6) (2001) 3068–3073, https://doi.org/10.1021/jf0013398.
[47] F. Li, X. Guan, C. Li, Effects of degree of milling on the starch digestibility of cooked rice during (in vitro) small intestine digestion, Int. J. Biol. Macromol. 188 (2021) 774–782, https://doi.org/10.1016/j.ijbiomac.2021.08.079.
[48] S. Fang, J. Wang, X. Xu, X. Zuo, Influence of low acyl and high acyl gellan gums on pasting and rheological properties of rice starch gel, Food Biophys. 13 (2) (2018) 116–123, https://doi.org/10.1007/s11483–018–9517–8.
[49] T. Wang, Y. Yang, W. Feng, R. Wang, Z. Chen, Co–folding of hydrophobic rice proteins and shellac in hydrophilic binary microstructures for cellular uptake of apigenin, Food Chem. October 2019 (309) (2019) 125695, https://doi.org/10.1016/j.foodchem.2019.125695.
[50] M.M. Heydari, T. Najib, V. Meda, Investigating starch and protein structure alterations of the processed lentil by microwave–assisted infrared thermal treatment and their correlation with the modified properties, Food Chem. Adv. 1 (2022) 100091, https://doi.org/10.1016/J.FOCHA.2022.100091.
[51] A. Barth, Infrared spectroscopy of proteins, Biochim. Biophys. Acta (BBA) Bioenergetics 1767 (9) (2007) 1073–1101, https://doi.org/10.1016/j.bbabio.2007.06.004.
[52] J. Kubelka, Multivariate analysis of spectral data with frequency shifts: application to temperature dependent infrared spectra of peptides and proteins, Anal. Chem. 85 (20) (2013) 9588–9595, https://doi.org/10.1021/ac402083p.
[53] N. Linlaud, E. Ferrer, M.C. Puppo, C. Ferrero, Hydrocolloid interaction with water, protein, and starch in wheat dough, J. Agric. Food Chem. 59 (2) (2011) 713–719, https://doi.org/10.1021/jf1026197.
[54] Y. Shen, G. He, W. Gong, X. Shu, D. Wu, N. Pellegrini, et al., Pre–soaking treatment can improve cooking quality of high–amylose rice while maintaining its low digestibility, Food Funct. 13 (23) (2022) 12182–12193, https://doi.org/10.1039/D2FO02056D.
[55] S. Wang, P. Li, J. Yu, P. Guo, S. Wang, Multi–scale structures and functional properties of starches from Indica hybrid, Japonica and waxy rice, Int. J. Biol. Macromol. 102 (2017) 136–143, https://doi.org/10.1016/J.IJBIOMAC.2017.04.020.
[56] S. Garg, N. Sharma, A. Kumari, M. Bala, R. Kaur, Impact of parboiling on nutritionally important starch fractions, pasting properties, and in vitro starch digestibility of rice genotypes, Cereal Res. Commun. 53 (1) (2025) 439–449, https://doi.org/10.1007/s42976–024–00547–x.
[57] Z. Nhouchi, E.P. Botosoa, C. Chèné, R. Karoui, Mid infrared as a tool to study the conformational structure of starch and proteins with oil addition during gelatinization, LWT 157 (2022) 113093, https://doi.org/10.1016/J.LWT.2022.113093.
[58] S. Dhital, V.M. Butardo, S.A. Jobling, M.J. Gidley, Rice starch granule amylolysis – differentiating effects of particle size, morphology, thermal properties and crystalline polymorph, Carbohydr. Polym. 115 (2015) 305–316, https://doi.org/10.1016/j.carbpol.2014.08.091.

[59] C. Kim, B. Yoo, Rheological properties of rice starch–xanthan gum mixtures, J. Food Eng. 75 (1) (2006) 120–128, https://doi.org/10.1016/j.jfoodeng.2005.04.002.
[60] K. Dome, E. Podgorbunskikh, A. Bychkov, O. Lomovsky, Changes in the crystallinity degree of starch having different types of crystal structure after mechanical pretreatment, Polymers 12 (3) (2020) 1–12, https://doi.org/10.3390/polym12030641.
[61] B. Yan, T. Chen, Y. Tao, N. Zhang, J. Zhao, H. Zhang, et al., Fabrication, functional properties, and potential applications of mixed gellan–polysaccharide systems: a review, Annu. Rev. Food Sci. Technol. 15 (1) (2024) 151–172, https://doi.org/10.1146/ANNUREV–FOOD–072023–034318.
[62] C. Peng, F. Wang, K. Nishinari, F. Jiang, M. Xiao, Direct visualization of the side–by–side self–assembly of high and low acyl gellan gum by AFM, Carbohydr. Polym. 354 (2025) 123325, https://doi.org/10.1016/J.CARBPOL.2025.123325.
[63] A. Xu, C. Wei, Comprehensive comparison and applications of different sections in investigating the microstructure and histochemistry of cereal kernels, Plant Methods 16 (1) (2020) 1–13, https://doi.org/10.1186/S13007–020–0558–X/FIGURES/6.
[64] B.A. Bugusu, B.R. Hamaker, B. Rajwa, Interaction of maize zein with wheat gluten in composite dough and bread as determined by confocal laser scanning microscopy, Scanning 24 (1) (2002) 1–5, https://doi.org/10.1002/SCA.4950240101.
[65] M.H. Ong, J.M.V. Blanshard, Texture determinants of cooked, parboiled rice. II: physicochemical properties and leaching behaviour of rice, J. Cereal Sci. 21 (3) (1995) 261–269, https://doi.org/10.1006/jcrs.1995.0029.
[66] W. Zhang, B. Cheng, X. Zeng, Q. Tang, Z. Shu, P. Wang, Physicochemical and digestible properties of parboiled black rice with different amylose contents, Front. Nutr. 9 (2022) 934209, https://doi.org/10.3389/FNUT.2022.934209.
[67] X. Lu, S. Kraithong, A. Theppawong, Y. Liu, P. Sangsawad, N. Bunyameen, et al., The multifunctional role of hydrocolloids in modulating retrogradation, starch hydrolysis, and the gut microbiota, Food Chem. 489 (2025) 144974, https://doi.org/10.1016/J.FOODCHEM.2025.144974.
[68] C.M. Rosell, W. Yokoyama, C. Shoemaker, Rheology of different hydrocolloids–rice starch blends. Effect of successive heating–cooling cycles, Carbohydr. Polym. 84 (1) (2011) 373–382, https://doi.org/10.1016/j.carbpol.2010.11.047.
[69] L.W. Meng, S.M. Kim, Effects of different carbohydrases on the physicochemical properties of rice flour, and the quality characteristics of fermented rice cake, Food Sci. Biotechnol. (2019), https://doi.org/10.1007/s10068–019–00693–7.
[70] X. Yin, X. Chen, J. Hu, L. Zhu, H. Zhang, Y. Hong, Effects of distribution, structure and interactions of starch, protein and cell walls on textural formation of cooked rice: a review, Int. J. Biol. Macromol. 253 (Pt 6) (2023), https://doi.org/10.1016/j.ijbiomac.2023.127403.
[71] Y. Zhang, F. Li, K. Huang, S. Li, H. Cao, J. Xie, et al., Structural changes of starch under different milling degrees affect the cooking and textural properties of rice, Food Chem. X 17 (2023) 100627, https://doi.org/10.1016/J.FOCHX.2023.100627.
[72] D. John, S. Sureshkumar, M. Raman, Type-2 diabetes and identification of major genetic determinants of glycemic index in rice – a review, Starch - Stärke 74 (2022) 2100277, https://doi.org/10.1002/star.202100277.
[73] K. Liu, J. Zheng, F. Chen, Effect of domestic cooking on rice protein digestibility, Food Sci. Nutr. 7 (2) (2019) 608–616, https://doi.org/10.1002/fsn3.884.
[74] G.P. Yadav, C.G. Dalbhagat, H.N. Mishra, Preparation of low glycemic rice and comparison of its physicochemical properties, cooking characteristics, starch digestibility and microstructure with raw rice (Swarna Cv), Food Sci. Eng. (2022) 30–43, https://doi.org/10.37256/FSE.4120231882.
[75] B. Gong, L. Cheng, R.G. Gilbert, C. Li, Distribution of short to medium amylose chains are major controllers of in vitro digestion of retrograded rice starch, Food Hydrocoll. 96 (2019) 634–643, https://doi.org/10.1016/j.foodhyd.2019.06.003.